# Solvent-free mechanochemical fabrication of acrylic acid grafted chitosan for effective Cr (VI) ion remediation

*Dissertation submitted to*

*Visvesvaraya National Institute of Technology, Nagpur*

*In partial fulfilment of the requirements for*

*The award of the degree*

**Master of Science**

**In**

**Chemistry**

***by***

**Jigarkumar Rajeshbhai Devpura (MS23CHM002)**

Under The Guidance of

**Prof. Anupama Kumar**

**Department of Chemistry**

**Visvesvaraya National Institute of Technology**

**Nagpur, 440010 (India)**

**May 2025**

# Solvent-free mechanochemical fabrication of acrylic acid grafted chitosan for effective Cr (VI) ion remediation

*Dissertation submitted to*

*Visvesvaraya National Institute of Technology, Nagpur*

*In partial fulfilment of the requirements for*

*The award of the degree*

**Master of Science**

**In**

**Chemistry**

***by***

**Jigarkumar Rajeshbhai Devpura (MS23CHM002)**

Under The Guidance of

**Prof. Anupama Kumar**

**Department of Chemistry**

**Visvesvaraya National Institute of Technology**

**Nagpur, 440010 (India)**

**May 2025**

**©Visvesvaraya National Institute of Technology (VNIT) 2025**

# Department of Chemistry

# Visvesvaraya National Institute of Technology, Nagpur

## Declaration

I, Jigarkumar Rajeshbhai Devpura, hereby declare that this dissertation entitled **"Solvent-free mechanochemical fabrication of acrylic acid grafted chitosan for effective Cr (VI) ion remediation"** is carried out by me in the Department of Chemistry of Visvesvaraya National Institute of Technology, Nagpur. The work is original and has not been submitted earlier, whole or in part for the award of any degree at this or any other university/institute.

**Jigarkumar Devpura**

Date

## Certificate

This is to certify that the dissertation titled **"Solvent-free mechanochemical fabrication of acrylic acid grafted chitosan for effective Cr (VI) ion remediation"** is submitted by Jigarkumar Rajeshbhai Devpura in partial fulfilment of the requirements for the award of the **Master of Science in Chemistry, VNIT Nagpur.** This is comprehensive, complete, and fit for final evaluation.

**Prof . Anupama Kumar**
Department of Chemistry
VNIT, Nagpur

**Prof. Sujit Kumar Ghosh**
Head, Department of Chemistry VNIT ,Nagpur
Date:

## Non-Plagiarism Certificate

It is certified that we have examined the M.Sc. dissertation titled **"Solvent-free mechanochemical fabrication of acrylic acid grafted chitosan for effective Cr (VI) ion remediation"** by Jigarkumar Rajeshbhai Devpura with the following anti-plagiarism tools.

This thesis has been checked using TURNITIN AND found within the limit as per HEC plagiarism policy and instructions issued from time to time.

**Prof. Anupama Kumar**
Department of Chemistry
VNIT, Nagpur

**Jigarkumar Devpura**
MS23CHM002
ID-30075

# ACKNOWLEDGEMENT

This research work has been undertaken as a part of the final year M.Sc. Chemistry curriculum. The primary objective of this project is to integrate theoretical knowledge with practical application, providing hands-on experience that complements our academic learning.

I am deeply grateful to Prof. Anupama Kumar, my project supervisor, for her invaluable support, insightful feedback, and unwavering encouragement throughout the course of this study. Her commitment to excellence and detailed guidance have played a crucial role in the successful completion of this project.

My sincere appreciation also goes to Ms. Manisha Verma, Ph.D. scholar, and all the members of the Chemistry department for their continuous assistance and guidance, which significantly contributed to enriching my understanding and refining my work.

I would also like to express my gratitude to all the faculty members of the Chemistry department for their indirect yet meaningful contribution towards the successful execution of this research.

Lastly, I would like to thank my family and friends for their constant support, encouragement, and kindness throughout this academic journey.

## Abstract

Mechanochemical synthesis is an environmentally friendly, solvent-free approach for chemical modifications, providing both efficiency and ecological advantages. This research outlines the synthesis of acrylic acid grafted chitosan (AA-g-CTS), produced through a solvent-free mechanochemical method, aimed at adsorbing hexavalent chromium Cr (VI) from wastewater. The grafting was achieved by co-grinding chitosan and acrylic acid with potassium persulfate serving as a free radical initiator. After synthesis, the AA-g-CTS was washed and dried. % Grafting and grafting efficiency were found to be 60 % and 123.52%, respectively. The compound was characterised by FTIR, XRD, BET, zeta potential, pHPZC and CHNS analysis. FTIR analysis verified the successful addition of acrylic acid on chitosan, while XRD analysis indicated a reduction in crystallinity compared to the original chitosan. The point of zero charge (pHpzc) and zeta potential analysis were useful in knowing the surface charge. The ability of AA-g CTS to adsorb Cr (VI) was assessed under different conditions, such as pH, contact duration, initial Cr (VI) concentration, and adsorbent dosage. The highest adsorption capacity recorded for Cr (VI) was 26.17 mg g-1 under optimized conditions, pH = 5, dose was 0.2 g, concentration was 100 ppm, and time was 180 minutes. The Data was fitted to various adsorption isotherm to get an insight about the mechanism for adsorption. The results indicate that AA-g-CTS has the potential to be a sustainable and effective material for the removal of Cr (VI) from contaminated or industrial wastewater.

**Table of Contents**

## CHAPTER 1 – INTRODUCTION


| Section | Title | Page No. |
|---|---|---|
| 1.1 | Introduction of Chitosan and Chitin | 2 |
| 1.2 | Source of Chitin | 3 |
| 1.3 | Extraction of Chitin | 4 |
| 1.3.1 | Chemical Extraction | 4 |
| | Demineralization Process | 4 |
| | Deproteinization Process | 5 |
| | Decolorization | 5 |
| 1.3.2 | Biological Extraction | 5 |
| | Enzymatic Demineralization | 6 |
| | Enzymatic Deproteinization | 6 |
| 1.4 | Preparation of Chitosan | 6 |
| 1.4.1 | Chemical and Biological Deacetylation of Chitin | 6 |
| 1.5 | Structure of Chitin and Chitosan | 7 |
| 1.5.1 | Structure of Chitin | 7 |
| 1.5.2 | Structure of Chitosan | 8 |
| 1.6 | Physicochemical Properties of Chitosan | 8 |
| 1.6.1 | Solubility | 8 |
| 1.6.2 | Degree of Deacetylation (DDA) | 8 |
| 1.6.3 | Molecular Weight (Mw) | 8 |
| 1.6.4 | Crystallinity | 9 |
| 1.6.5 | pH Sensitivity | 9 |
| 1.6.6 | Hydrophilicity | 9 |
| 1.6.7 | Thermal Stability | 9 |
| 1.6.8 | Mechanical Properties | 10 |

| | | |
|---|---|---|
| 1.7 | Chitosan Derivatives and Applications | 10 |
| 1.7.1 | Quaternized and N-Alkyl Chitosan | 10 |
| 1.7.2 | Highly Cationic Chitosan | 10 |
| 1.7.3 | Hydroxyalkyl Chitosan | 11 |
| 1.7.4 | Carboxyalkyl Chitosan | 11 |
| 1.7.5 | Sugar Modification | 11 |
| 1.7.6 | Acylation Chitosan | 11 |
| 1.7.7 | Thiolated Chitosan | 12 |
| 1.7.8 | Sulfated and Phosphorylated Chitosan | 12 |
| 1.7.9 | Miscellaneous Chitosan Derivatives | 12 |
| 1.8 | Introduction of Acrylic Acid | 12 |
| 1.8.1 | Why Choose Acrylic Acid for Grafting? | 13 |
| 1.9 | Introduction of Mechanochemistry | 13 |
| 1.9.1 | Definition and Historical Background | 13 |
| 1.9.2 | Mechanisms and Fundamental Principles | 14 |
| 1.10 | Mechanochemical Techniques | 15 |
| 1.10.1 | Ball Milling | 15 |
| 1.10.2 | Extrusions | 16 |
| 1.10.3 | Shear Grinding | 17 |
| 1.10.4 | Reactive Milling | 17 |
| 1.10.5 | Mechanochemical Cocrystallization | 17 |
| 1.11 | Applications Across Various Fields | 17 |
| 1.12 | Application of Derivatized Chitosan | 18 |
| 1.12.1 | Biomedical Applications | 18 |
| 1.12.2 | Pharmaceutical and Nutraceutical | 19 |
| 1.12.3 | Environmental and Industrial Applications | 19 |
| 1.12.4 | Emerging Advanced Composites | 19 |
| 1.13 | Purpose of Study | 20 |
| 1.14 | Hexavalent Chromium (Cr VI) as an Environmental Pollutant | 20 |

## CHAPTER 2 MATERIALS AND METHOD


| Section | Title | Page No. |
|---|---|---|
| 2.1 | Chemicals Used | 23 |
| 2.2 | Preparation of Acrylic Acid Grafted Chitosan (AA-g-CTS) by Conventional Method | 23 |
| 2.3 | Preparation of Acrylic Acid Grafted Chitosan (AA-g-CTS) by Mechanochemical Method | 24 |
| 2.4 | Grafting Efficiency (%) and Percent Grafting (%) | 24 |
| 2.5 | Procedure for pH / pHzpc Analysis | 25 |
| 2.6 | Establishing Calibration for Potassium Dichromate ($K_2Cr_2O_7$) | 25 |
| 2.7 | Optimization of Adsorption Parameters | 26 |
| 2.8 | Adsorption Isotherms | 26 |
| 2.9 | Instrumentation | 27 |


## CHAPTER 3 – RESULTS AND DISCUSSION


| Section | Title | Page No. |
|---|---|---|
| 3.1 | Calculation of Grafting Efficiency (GE) and Percent Grafting (%G) | 32 |
| 3.2 | Characterization of Acrylic Acid-Grafted Chitosan (AA-g-CTS) | 32 |
| 3.2.1 | FTIR | 32 |
| 3.2.2 | XRD | 34 |
| 3.2.3 | BET | 35 |
| 3.3 | Zeta Potential | 36 |
| 3.4 | Point of Zero Charge (pHzpc) | 37 |
| 3.5 | Calibration Curve of $K_2Cr_2O_7$ | 38 |

| | | |
|---|---|---|
| 3.6 | Adsorption Properties | 40 |
| 3.6.1 | Effect of Dose | 40 |
| 3.6.2 | Effect of Time | 41 |
| 3.6.3 | Effect of pH | 42 |
| 3.6.4 | Effect of Concentration | 43 |
| 3.6 | Adsorption Isotherm Models | 44 |


**CHAPTER 4 - CONCLUSION**


| Section | Title | Page No. |
|---|---|---|
| 4.1 | Conclusion | 49 |
| — | References | 50 |


**LIST OF FIGURES**

**CHAPTER -1 INTRODUCTION**


| Figure No. | Title | Page No. |
|---|---|---|
| Fig. 1.1 | Source of Chitin | 3 |
| Fig. 1.2 | Structure of Chitin | 7 |
| Fig. 1.3 | Structure of Chitosan | 8 |
| Fig. 1.4 | Structure of Acrylic Acid | 13 |
| Fig. 1.5 | Diagram of Ball Milling | 15 |
| Fig. 1.6 | Diagram of Planetary Ball Mills | 16 |
| Fig. 1.7 | Diagram of Vibratory Ball Mills | 16 |


**Chapter 2: Materials and Methods**


| Figure No. | Title | Page No. |
|---|---|---|
| Fig. 2.1 | FTIR Instrument | 28 |

| | | |
|---|---|---|
| Fig. 2.2 | Powder X-ray Diffractometer | 29 |


**Chapter 3: Results and Discussion**


| Figure No. | Title | Page No. |
|---|---|---|
| Fig. 3.1 | FTIR spectra of (a) CTS, (b) acrylic acid, (c) AA-g-CTS (solution method), (d) AA-g-CTS (mechanochemical method) | 32 |
| Fig. 3.2 | XRD patterns of (A) Acrylic acid, (B) Chitosan, (C) Acrylic acid grafted chitosan | 35 |
| Fig. 3.3 | (a) BET analysis of AA-g-CTS (b) BJH analysis of AA-g-CTS | 36 |
| Fig. 3.4 | Show ( a) Zetapotential (b) Zetapotential Vs pH | 37 |
| Fig. 3.5 | Point of zero charge of AA-g-CTS | 38 |
| Fig. 3.6 | UV data of standard Potassium dichromate ($K_2Cr_2O_7$) | 39 |
| Fig 3.7 | Calibration graph of standard Potassium dichromate ($K_2Cr_2O_7$) | 39 |
| Fig. 3.8 | Impact of dose on the adsorption of Cr(VI) onto the AA-g-CTS | 40 |
| Fig. 3.9 | Impact of time on the adsorption of Cr(VI) onto the AA-g-CTS | 42 |
| Fig. 3.10 | Impact of pH on the adsorption of Cr(VI) onto the AA-g-CTS | 43 |
| Fig. 3.11 | Impact of concentration on the adsorption of Cr(VI) onto the AA-g-CTS | 44 |
| Fig. 3.12 | Langmuir isotherm plot | 45 |
| Fig. 3.13 | Freundlich isotherm plot | 46 |
| Fig. 3.14 | Temkin isotherm plot | 47 |


**List of Tables**


| Table No. | Title | Page No. |
|---|---|---|
| Table 2.1 | Chemicals used | 23 |
| Table 3.1 | Grafting efficiency and Percent grafting | 32 |
| Table 3.2 | BET and BJH data | 36 |
| Table 3.3 | Langmuir model data | 45 |
| Table 3.4 | Freundlich model data | 46 |

| | | |
|---|---|---|
| Table 3.5 | Temkin model data | 47 |

# CHAPTER - 1

# INTRODUCTION

Chitin and Chitosan Compound: Properties, Application, and Prospects

## 1.1 Introduction

Chitin is recognized as the second most abundant biopolymer on the planet, surpassed only by cellulose. It is a polysaccharide formed from β(1→4)-linked units of 2-acetamido-2-deoxy-β-D-glucose, also known as N-acetylglucosamine. While structurally similar to cellulose, chitin differs due to the presence of acetamide groups attached at the C-2 positions*[1]*.

Chitosan is produced by the N-deacetylation of chitin, resulting in a linear polymer composed of α(1→4)-linked 2-amino-2-deoxy-β-D-glucopyranose units. This transformation makes chitosan a unique and adaptable material for various uses*[2]*.

Chitin is a rigid, white, nitrogen-containing polysaccharide found in the exoskeletons and internal structures of invertebrates. The waste generated from these natural polymers significantly contributes to surface pollution in coastal regions. Extracting chitosan from crustacean shells, which are a byproduct of the food industry, is both cost-effective and sustainable, particularly when carotenoids are also recovered during the process. These shells are rich in astaxanthin, a carotenoid that cannot yet be synthesized. They are widely used in aquaculture as a fish feed additive, especially for salmon farming*[3]*.

In India, the chitinous waste generated from shellfish is estimated to range between 60,000 and 80,000 tons annually. With three sides of the country bordered by oceans and abundant inland water resources like ponds, lakes, and lagoons, India holds immense potential for aquaculture. Advancing research in chitin and chitosan can significantly contribute to the nation's economic growth and academic development.

Chitin and chitosan are now commercially manufactured in countries such as India, Poland, Japan, the United States, Norway, and Australia. Globally, including in India, substantial research efforts are underway to develop and enhance the functionalities of chitin and chitosan, aiming to expand their applications and maximize their utility*[4]*.

## 1.2 Sources of Chitin

Chitin is primarily sourced from the exoskeletons of arthropods and various other biological materials that contain chitin, including crustaceans, insects, and certain fungi. These substances generally consist of 30–40% protein, 30–50% calcium carbonate, and 20–30% chitin *[5]*. In terms of structure, chitin represents a well-organized biological nanocomposite characterized by a unique hierarchical design. At the smallest level, the structure is made up of chitin polysaccharide chains that create slender, elongated crystalline structures. These structures are enveloped by protein layers, resulting in nanofibrils that are roughly 2–5 nm in diameter and about 300 nm long. Multiple nanofibrils come together to form larger chitin-protein fibers that vary in diameter from 50 to 300 nm *[6]*.

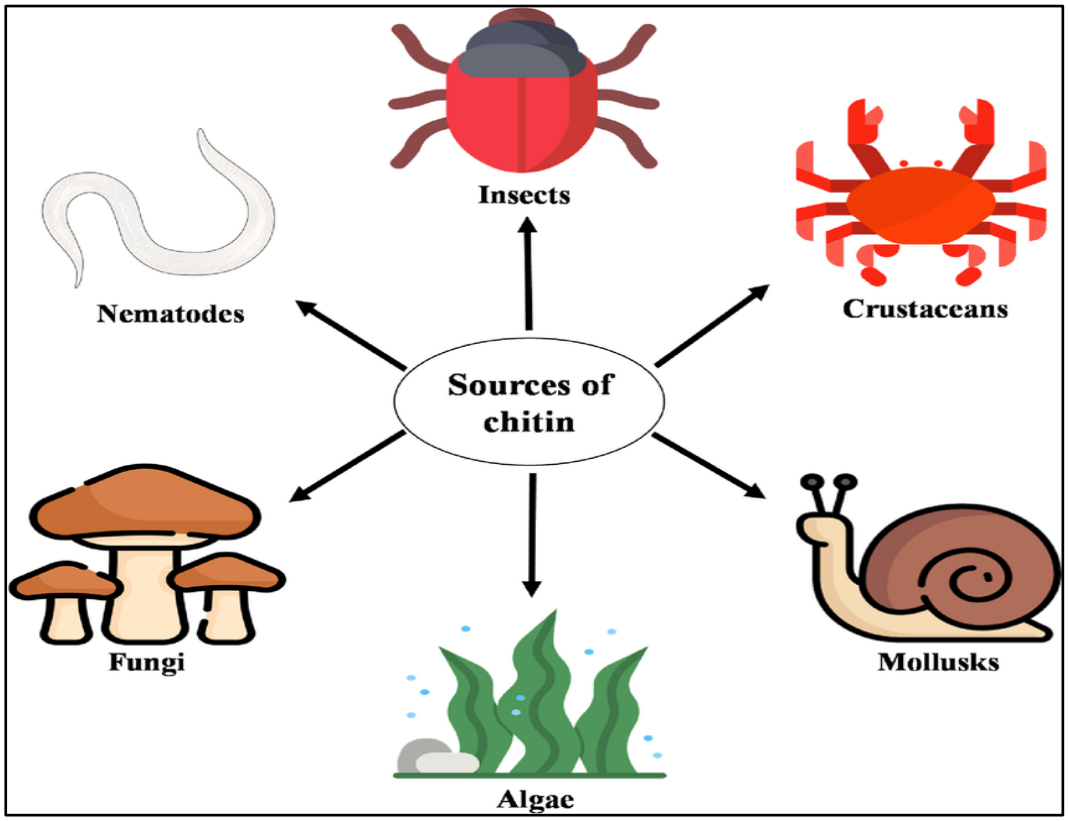


**Fig. 1.1 Source of Chitin**

Chitin can be classified into three primary allomorphic forms: α-chitin, β-chitin, and γ-chitin. In α-chitin, the molecular chains are arranged parallel to one another within stacked sheets along the c-axis, and this type is most frequently found in the exoskeletons of marine crustaceans such as lobsters, crabs, and shrimp. β-chitin exhibits an antiparallel arrangement of sheets along the same axis and is typically present in squid pens, certain

diatoms, and particular deep-sea worms (vestimentiferans). γ-chitin features a more intricate arrangement, where every third sheet is oriented in the opposite direction to the prior two. This form is mainly linked to fungal species and yeasts*[7]*.

## 1.3 Extraction of Chitin

Cuticles of various crustaceans like crabs, shrimps, lobsters, and fish scales are the major sources of chitin. Crustaceans carry an exoskeleton of proteins, chitin, and calcium carbonate, which bind together to form an external shell. Protein and chitin bind together, and a small part of the protein is available in the polymer complex. Hence, chitin's separation from the shell requires the elimination of two major constituents, protein and minerals*[8]*. A deproteinization process removes protein, a deproteinization process removes minerals, and a demineralization process removes minerals. In some cases, an additional process of decolorization is carried out to remove pigments. A variety of methods have been adopted to produce chitin. Moreover, among the two methods, the biological method offers some advantages, specifically in the time consumption and quality of chitin produced. Therefore, extraction always begins by choosing crustacean shells. For any particular separation, shells of identical size and species are preferred. In the case of shrimp shells, separation is easier due to the thinner shell wall, but the yield is lower compared to crab and lobster, allowing for a higher quality of chitin to be recovered. Thus, the availability of crustaceans remains a key factor for the extraction of chitin*[9]*

### 1.3.1 Chemical Extraction

Demineralization Process

The extraction of minerals such as calcium carbonate and calcium phosphate from shells is achieved through an acid-based approach. Commonly utilized acids for this procedure include hydrochloric acid (HCl), nitric acid ($HNO_3$), sulfuric acid ($H_2SO_4$), acetic acid (CH3COOH), and formic acid (HCOOH). After the acid treatment, the shells undergo vacuum filtration and are rinsed with distilled water for about 30 minutes until the pH reaches neutrality. The demineralized shells are subsequently dried at 60ºC for 24 hours.

Calcium carbonate can be broken down into calcium chloride with the help of hydrochloric acid, which also releases water and carbon dioxide. Additionally, other minerals and acid combine to create soluble salts, which are then removed via filtration. Following a

thorough washing with distilled water and drying, chitin is extracted. A number of variables, including as shell type, extraction time, temperature, particle size, acid content, and the solute-to-solvent ratio, affect the demineralization process. Stoichiometry is used to calculate the ratio, which states that one mole of calcium carbonate requires two moles of acid to break down. Higher temperatures enhance the solvent's ability to penetrate the chitin matrix, which is also impacted by particle size. But long-term exposure to high temperatures, strong acids, and lengthy processing times can all harm the characteristics of chitin*[10]*.

### Deproteinization Process

After the demineralization process, proteins are removed using an alkaline treatment with agents such as sodium hydroxide (NaOH), potassium hydroxide (KOH), calcium hydroxide ($Ca(OH)_2$), sodium carbonate ($Na_2CO_3$), potassium carbonate ($K_2CO_3$), sodium bicarbonate ($NaHCO_3$), and various other alkaline substances. Deproteinization is generally conducted with NaOH or KOH through continuous stirring for about two hours at 90ºC. The mixture is subsequently filtered under vacuum and washed with distilled water until a neutral pH is reached. The deproteinized shells are then dried at 60ºC for a duration of 24 hours. Throughout this procedure, the connection between the protein and chitin is disrupted. However, both NaOH and KOH can potentially lead to the degradation and depolymerization of chitin. The conditions for deproteinization can differ based on the type of crustaceans being processed, and alkaline treatment may result in partial deacetylation and a reduction in the molecular weight of chitin*[10]*.

### Decolorization.

The final stage in the refinement of chitin is decolorization, which involves the removal of pigments utilizing organic solvents like acetone. Typically, this procedure requires soaking in acetone for 10 to 20 minutes and then allowing it to dry at room temperature for roughly two hours.

### 1.3.2 Biological Extraction

The extraction of chitin through chemical methods poses environmental issues because of the use of toxic substances, significant energy usage, and the production of waste. On the other hand, biological extraction offers a more eco-friendly option. This technique

minimizes the environmental effects linked to acidic and alkaline processes while ensuring a uniform quality of chitin. However, the biological method also has its drawbacks, such as lower chitin solubility and extended processing durations*[11]*.

### Enzymatic demineralization

The shells of crustaceans contain minerals and proteins that can be dissolved by organic acids generated by microorganisms like lactic acid bacteria. During the process of enzymatic demineralization, organic acids engage with calcium carbonate found in the shells, leading to the formation of calcium salts that precipitate. These salts were meticulously isolated from the culture medium and subjected to washing. The retrieved salts may be utilized as preservatives and anti-icing agents*[12]*.

### Enzymatic Deproteinization

Enzymatic deproteinization employs proteolytic enzymes like alcalase, papain, pancreatin, pepsin, and trypsin to break down proteins. These enzymes can be obtained from various sources including plants, microorganisms, and animals. Alcalase, a serine endopeptidase from Bacillus licheniformis, is frequently utilized because of its specificity for hydrophobic amino acids at the terminal positions. It is preferred for the production of chitin, protein hydrolysates, and for astaxanthin recovery, as it reduces bitterness and allows for controlled hydrolysis. Following enzymatic deproteinization, the shell is subjected to demineralization with hydrochloric acid (HCl). Nonetheless, chitin extracted through enzymatic processes tends to have a higher residual protein content compared to that obtained via alkaline methods*[12]*.

## 1.4 Preparation of Chitosan

Chitosan is derived from chitin, a naturally occurring polysaccharide found in the exoskeletons of crustaceans such as shrimp, crabs, and lobsters. The extraction process involves multiple steps, including demineralization, deproteinization, and deacetylation.

### 1.4.1 Chemical and Biological Deacetylation of Chitin

Chitin undergoes deacetylation through acid or alkali treatment. The process can be homogeneous or heterogeneous. In homogeneous deacetylation, chitin is treated with concentrated alkali at 25ºC for three hours, followed by dispersion in compressed ice

at approximately 0ºC. In heterogeneous deacetylation, hot concentrated alkali is applied, and the material is subsequently rinsed with distilled water until neutrality is achieved. Achieving a high degree of deacetylation is challenging, but incorporating thiophenol as a catalyst can help reduce degradation through oxygen sequestration and improve reaction efficiency*[13]*.

For effective deacetylation, the alkaline concentration must be four times the total amino group content in the polysaccharide. The reaction is typically conducted at 100ºC for one hour. Lower alkali concentrations and shorter exposure times are recommended to prevent polymer degradation.

Despite its efficiency, chemical deacetylation has drawbacks, including high energy consumption and environmental concerns. Enzymatic deacetylation has been explored to address these issues. Enzymes such as chitin deacetylation act as catalysts to hydrolyze N-acetamide bonds and can be derived from fungi such as Muor rouxii, Absidia coerulea, Aspergillus nidulans, and celletotrichum lindemuthianum. These enzymes exhibit thermal stability and strong affinity for β-(1,4)-linked N-acetyl-D-glucosamine polymer. Enzymatic deacetylation can be conducted in batch or continuous cultures, with batch processes yielding lower molecular weight chitosan over time*[14]*.

## 1.5 Structure of Chitin and Chitosan

### 1.5.1 Structure of Chitin

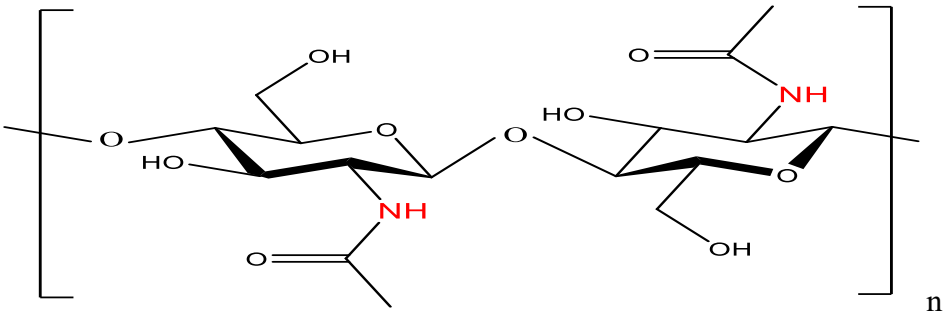


**Fig. 1.2 Structure of Chitin**

### 1.5.2 Structure of Chitosan

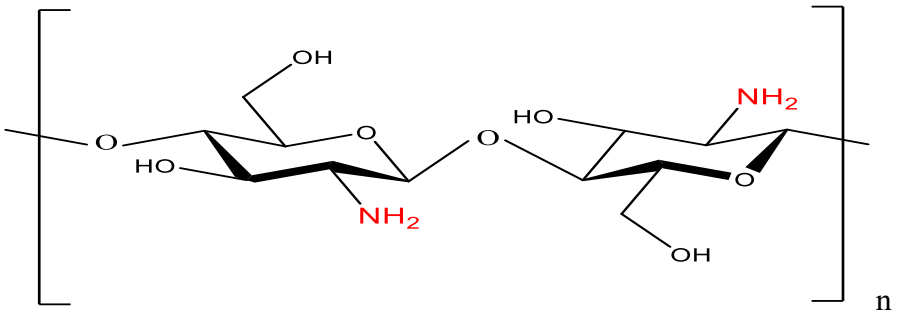


**Fig. 1.3 Structure of Chitosan**

## 1.6 Physicochemical Properties of Chitosan

Chitosan, a biopolymer derived from chitin, exhibits a distinct set of physicochemical properties that contribute to its widespread applicability. These attributes are fundamental in determining its suitability across various fields, including biomedical engineering, pharmaceuticals, and environmental science.

### 1.6.1 Solubility

One key feature of chitosan is its ability to dissolve in acidic conditions. This phenomenon happens because its amino group becomes protonated, which boosts its interactions with water molecules and eases its dissolution in solutions with a pH lower than 6.5. Various factors affect solubility, such as the degree of deacetylation (DDA) and molecular weight (Mw). Generally, a higher DDA and a lower Mw improve solubility by reducing intermolecular interactions.

### 1.6.2 Degree of Deacetylation (DDA)

The degree of deacetylation significantly affects chitosan`s physicochemical behaviours. It refers to the percentage of the N-acetyl group removed during the deacetylation process. A higher DDA translates to more free amino groups, improving solubility, reactivity, and biological functionality. Generally, chitosan with a DDA of more than 70% is deemed suitable for a majority of applications.

### 1.6.3 Molecular Weight (Mw)

Chitosan`s molecular weight has a direct impact on its functional properties. Low molecular weight chitosan tends to be more soluble and reactive due to reduced intermolecular interactions, making it ideal for applications such as drug delivery and water purification. On the other hand, high molecular weight chitosan provides increased viscosity and mechanical strength, which is beneficial for applications like biodegradable packaging and tissue engineering scaffolds. The selection of Mw depends on the specific requirements of each application.

### 1.6.4 Crystallinity

Compared to its precursor, chitin, chitosan exhibits lower crystallinity due to structural changes occurring during the deacetylation process. The removal of the acetyl group disrupts the molecular alignment, resulting in a more amorphous structure. This decrease in crystallinity affects mechanical properties and overall stability. Factors such as Mw and DDA influence crystallinity, higher DDA and lower Mw typically reduce crystallinity, enhancing solubility and reactivity, but potentially diminishing mechanical robustness.

### 1.6.5 pH Sensitivity

Chitosan demonstrates pH-responsive behaviours owing to its polycationic nature. In acidic conditions, protonation of its amino groups leads to increased solubility and charge density. However, as the pH rises, deprotonation occurs, causing a decrease in solubility and surface charge. This pH-sensitive property makes chitosan particularly useful in controlled drug release systems, where the release of therapeutic agents can be modulated by pH variations.

### 1.6.6 Hydrophilicity

The hydrophilic nature of chitosan is attributed to the presence of amino and hydroxyl functional groups, which enable strong interactions with water. This property allows chitosan to form hydrogels, a three-dimensional polymer network capable of retaining substantial amounts of water. Hydrogels are widely utilized in biomedical applications, including wound dressing and tissue scaffolds, where they create a hydrated environment conducive to healing and cell growth.

### 1.6.7 Thermal stability

Chitosan exhibits considerable thermal stability, although its degradation temperature varies based on factors such as DDA and Mw. A higher DDA and lower Mw generally correlate with reduced thermal resistance due to weakened intermolecular bonding. Thermal stability is an essential factor for application involving high-temperature processes, such as sterilization and composite material fabrication.

### 1.6.8 Mechanical Properties

Chitosan can be processed into various structural forms, including films, fibres, and scaffolds, with tunable mechanical properties. These properties are influenced by molecular weight, deacetylation level, and the incorporation of cross-linking agents. In tissue engineering, chitosan scaffolds are designed to mimic the mechanical characteristics of biological tissues, ensuring structural support for cellular attachment and differentiation. Similarly, in the packaging industry, chitosan-based films can be tailored to achieve a desirable balance between flexibility and durability, making them an environmentally friendly alternative to conventional packaging materials*[15]*.

## 1.7 Chitosan Derivatives and Their Applications

Chitosan, a biopolymer obtained from chitin, is renowned for its compatibility with biological systems, environmental breakdown, and versatility. Chemical modification can enhance its solubility, antimicrobial properties, and mechanical strength. These transformations render chitosan derivatives particularly beneficial in the field of pharmaceuticals, biomedicine, environmental science, and various industries. Researchers have modified its structure to create specific derivatives possessing distinct properties for a wide range of applications*[16]*.

### 1.7.1 Quaternized and N-Alkyl chitosan

Quaternized and N-alkyl chitosan derivatives are altered to enhance solubility, antimicrobial effectiveness, and mucoadhesive properties. Introducing quaternary ammonium groups boosts the polymer`s positive charge, improving its interaction with biological membranes. These derivatives are found to be extensively used in drug and gene delivery systems, wound healing, and antimicrobial coatings. Moreover, they can form stable complexes with nucleic acids, positioning them as promising options for controlled drug release and gene therapy*[17]*.

### 1.7.2 Highly Cationic Chitosan

Highly cationic chitosan derivatives are characterized by a high positive charge density, which increases bioadhesion. This trait makes them particularly effective for enhancing drug absorption, immobilizing enzymes, and formulating cosmetics. Their strong affinity for negatively charged cellular surface renders them ideal for targeted drug delivery, tissue engineering, and antibacterial treatments. Research is also investigating their application in ophthalmic drug formulations and oral vaccines to boost bioavailability.

### 1.7.3 Hydroxyalkyl Chitosan

Hydroxyalkyl chitosan derivatives, produced using epoxides like ethylene oxide or propylene oxide, display enhanced solubility, viscosity, and the ability to form films. These characteristics make them suitable for use in hydrogels, wound dressings, tissue engineering scaffolding, and as drug carriers involving nanoparticles. Their hydrophilic nature promotes cell adhesion and growth, making them important in regenerative medicine and biomedical coatings.

### 1.7.4 Carboxyalkyl Chitosan

Carboxyalkyl chitosan derivatives introduce amphoteric characteristics that allow for charge modulation, which aids in pH-sensitive drug delivery, bone regeneration, and antimicrobial uses. These derivatives are commonly utilized in the chelation of metal ions, water purification, and protein-based drug delivery systems. Their ability to form hydrogels has also broadened their application in wound healing and tissue scaffolding*[18]*.

### 1.7.5 Sugar-Modified Chitosan

Sugar-modified chitosan derivatives are functionalized with sugar molecules to improve biocompatibility and facilitate selective targeting of cells. These derivatives are especially beneficial for drug delivery targeting the liver, immune cell targeting, and engineering tissue scaffolds. Galactosylated Chitosan is notably researched for its capacity to bind with hepatocyte receptors, while mannosylated chitosan is studied for its potential in vaccine delivery and enhancing immune responses.

### 1.7.6 Acylation Chitosan

Acylation of chitosan derivatives, which include both N-acyl and O-acyl modifications, shows increased hydrophobicity and mechanical strength. These attributes make them appropriate for membrane technology, extended-release drug formulation, and textile applications. They are critical in developing water-resistant coatings, antibacterial surfaces, and biodegradable packaging materials*[18]*.

### 1.7.7 Thiolated Chitosan

Thiolated chitosan derivatives contain sulfhydryl(-SH) groups, which enhance mucoadhesion and bioavailability. This feature makes them suitable for use in mucoadhesive drug delivery, wound healing, and enzyme immobilization. The capacity of Thiolated chitosan to form disulfide bonds with mucosal surfaces prolongs drug retention, offering significant benefits in ophthalmic, nasal, and buccal drug formulations.

### 1.7.8 Sulfated and phosphorylated chitosan

Sulfated and phosphorylated chitosan derivatives are enhanced with sulfate and phosphate groups, improving anticoagulant properties and binding metals. Current research on sulfated chitosan includes its potential in blood-compatible biomaterials, tissue engineering, and anti-inflammatory applications. Phosphorylated chitosan, known for its strong affinity to calcium ions, is valuable for bone regeneration, dental coatings, and water treatment processes.

### 1.7.9 Miscellaneous Chitosan Derivatives

Various specialized Chitosan derivatives exist, such as azidated Chitosan suited for click chemistry, EDTA-chitosan designed for metal ion chelation, and fluorinated chitosan intended for hydrophobic coatings. These modifications broaden their use in biomedical implants, catalysts, and functional coatings. Additionally, enzymatically modified chitosan derivatives are being explored for targeted drug delivery and enhanced biocompatibility in medical uses.

## 1.8 Introduction of Acrylic Acid

Acrylic acid ($C_3H_4O_2$) is a simple organic compound that contains both a carboxylic acid group and a vinyl group. It is typically found as a colorless, corrosive liquid with a sharp odor and is known for its high reactivity, These functional groups enable it to undergo

polymerization and chemical grafting, making it a widely used monomer in materials science and polymer chemistry.

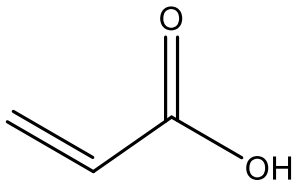


**Fig 1.4 structure of Acrylic acid**

In the context of biopolymer modification, acrylic acid plays a significant role due to its ability to introduce a carboxyl group onto the polymer backbone. When grafting onto chitosan, it can improve properties such as hydrophilicity, ion exchange capacity, and surface reactivity. Drug delivery systems and catalysis. Additionally, acrylic acid supports green synthesis approaches like mechanochemistry, which reduce or eliminate the use of harmful solvents and reaction conditions*[19]*.

### 1.8.1 Why do we choose acrylic acid for grafting?

The selection of acrylic acid for study is based on its efficiency in modifying biopolymers like chitosan through the introduction of carboxylic functional groups. These modifications contribute to improved physicochemical properties such as enhanced water compatibility, adsorption potential, and chemical stability. Furthermore, acrylic acid is economically feasible, readily available, and compatible with sustainable techniques such as mechanochemical synthesis. These characteristics make it an excellent choice for developing advanced chitosan-based materials with a wide range of potential applications.

## 1.9 Introduction to Mechanochemistry

### 1.9.1 Definition and Historical Background

Mechanochemistry is the branch of chemistry that harnesses mechanical energy, such as grinding, milling, or shearing, to drive chemical transformation instead of relying on traditional heat- or solvent-based methods. The concept dates back to early experimental observation by Micheal Faraday in 1820, who demonstrated that mechanically grinding silver chloride with zinc powder reduced AgCl to metallic silver*[20]*. Later, Wilhelm Ostwald formally recognized mechanochemistry as a

distinct discipline in 1907, categorizing it alongside electrochemistry, photochemistry, and thermochemistry*[21]*. Over the last few decades, mechanochemical synthesis has gained significant attention for its efficiency, sustainability, and ability to induce unique reaction pathways, which are often unattainable in conventional synthetic approaches*[22]*.

Mechanochemistry has evolved significantly, moving beyond its initial applications in metallurgy and solid-state chemistry to encompass areas such as pharmaceuticals, material science, and environmental chemistry. The method's ability to facilitate reaction under solvent-free conditions makes it a vital tool for green chemistry, reducing waste and energy consumption while enhancing reaction efficiency*[23]*. With recent technological advancements, mechanochemistry is now a promising alternative to traditional synthesis routes, particularly for complex materials and biologically relevant molecules.

### 1.9.2 Mechanisms and Fundamental Principles

Mechanochemical reactions occur due to the absorption of mechanical energy, which facilitates molecular transformation through bond cleavage and reformation. This energy is typically imparted via high-energy ball milling, extrusion, or simple grinding, leading to a variety of physical and chemical effects, including particle size reduction, formation of surface defects, and localized increases in pressure and temperature *[20]*. These phenomena contribute to enhanced reactivity, enabling reaction to proceed in solid-state conditions, eliminating or significantly reducing the need for solvent- thereby aligning mechanochemistry with sustainable and environmentally friendly practices*[23]*.

Several theoretical models have been proposed to explain mechanochemical transformations:

- The hot-spot theory postulates that intense localized heat generated during milling initiates chemical reactions.
- The magma-plasma model suggests that extreme shear forces and transient plasma states facilitate bond cleavage.

- The pseudo-fluid model considers mechanochemical systems as dynamic, high-energy fluid-like states during processing *[22]*.

Additionally, a mechanic

Chemical processes often exhibit reaction pathways distinct from those observed in solution-based chemistry. The unique energy input can lead to the formation of metastable intermediates, alternative product distribution, and increased reaction compared to conventional approaches. Understanding these mechanisms continues to be an area of active research, with computational simulation and in-situ monitoring techniques playing a critical role in unraveling the complexities of mechanochemical transformations *[22]*.

## 1.10 Mechanochemical Techniques

Several techniques are used in mechanochemistry to induce chemical transformation efficiently:

### 1.10.1 Ball Milling

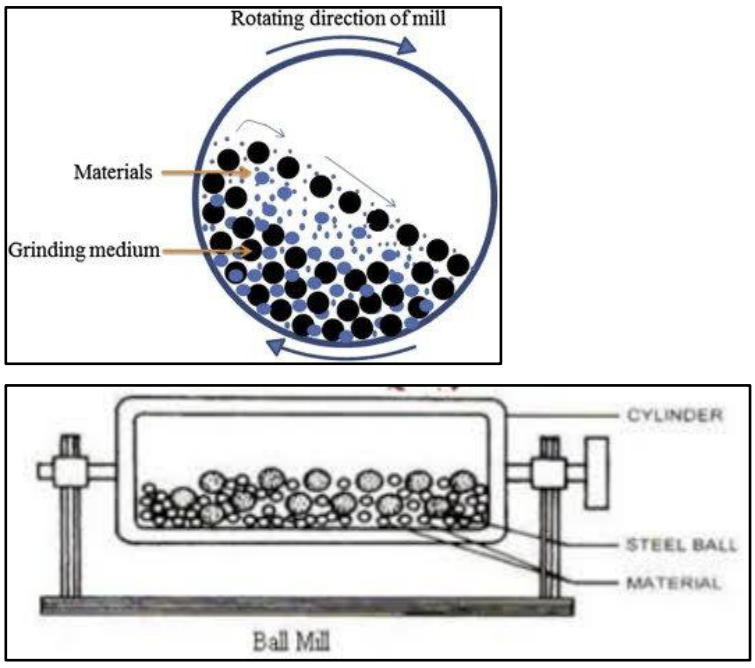


**Fig 1.5 Diagram of Ball milling**

One of the most widely employed techniques is where mechanical force is applied using rotating or oscillating milling jars containing milling balls. This method provides localized energy drive reactions*[24]*. Various types of ball mills include:

**Planetary ball mills:** High-energy mills where grinding balls are subjected to centrifugal force, enhancing reaction efficiency.

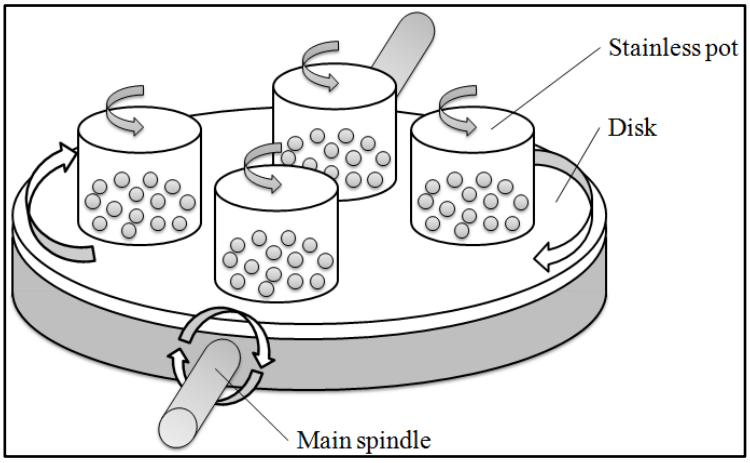


**Fig 1.6 Diagram of Planetary ball mills**

**Vibratory ball mills:** Generate energy through oscillation, useful for small-scale synthesis.

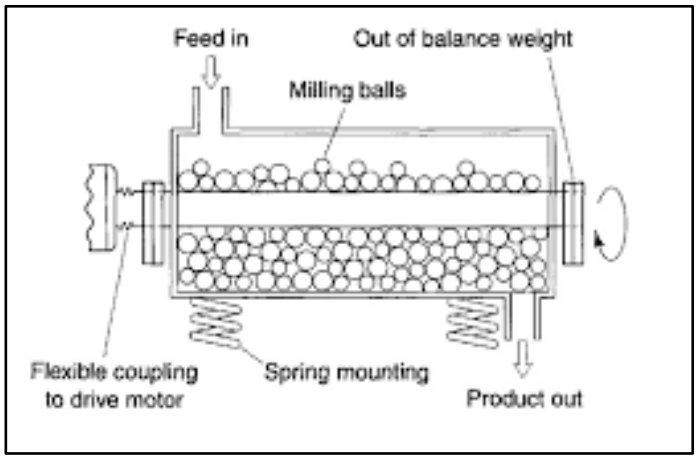


**Fig 1.7 Diagram of Vibratory ball mills**

**Attritor mills:** Used for continuous mechanochemical reaction with controlled energy input.

### 1.10.2 Extrusion

A continuous mechanochemical approach where reactants are subjected to mechanical shearing under controlled pressure. Extrusion is widely applied in polymer synthesis and pharmaceutical applications due to its scalability and minimal solvent usage*[25]*.

### 1.10.3 Shear Grinding

A technique in which reactants are ground together using a mortar and pestle or in a twin-screw extruder to enhance solid-state reactions. This method is beneficial for organic reactions that require gentle mechanical activation.

### 1.10.4 Reactive Milling

Reactive milling involves the simultaneous mechanical activation and chemical reaction of solid reactants. This is commonly used in materials science for synthesizing alloys, intermetallics, and ceramic materials under controlled atmosphere conditions.

### 1.10.5 Mechanochemical cocrystallization

Mechanochemical cocrystallization is widely utilized in the pharmaceutical industry to enhance drug solubility, stability, and bioavailability. It involves grinding two or more solid components together to form a new crystalline phase with enhanced properties*[26]*.

## 1.11 Application Across Various Fields

Mechanochemical has proven to be a versatile tool with wide-ranging applications:

- Material Science: It is extensively used for synthesizing advanced materials such as metal-organic frameworks (MOFs), nanostructured catalysts, and high-surface-area oxides.
- **Organic Synthesis:** Mechanochemistry enables solvent-free organic transformations, including cross-coupling reactions, oxidation coupling, and enantioselective processes*[20]*.
- **Polymer Chemistry:** The mechanochemical production of linear and porous polymer has emerged as an innovative alternative to conventional polymerization techniques, overcoming issues related to solubility and rapid precipitation*[27]*.
- **Pharmaceutical industry:** Mechanochemical strategies have revolutionized the formulation of pharmaceutical cocrystals, improving drug solubility and bioavailability *[23]*.

- **Catalysis:** The application of mechanochemical in heterogeneous catalysis has allowed for the synthesis of highly active catalysts, facilitating defect engineering and enhanced surface properties.
- **Environmental Chemistry:** Mechanochemical approaches are being explored for waste remediation, carbon capture, and the degradation of persistent pollutants, contributing to sustainability efforts*[27]*.

**Innovations and Future Prospects.** Recent advancements in mechanochemistry involve integrating mechanical energy with alternative energy sources such as ultrasound, photochemistry, and electrochemistry, collectively termed "mechanochemistry 2.0". This hybrid approach expands the potential of mechanochemical reactions, enabling precise control over activation energy and facilitating the development of novel synthetic routes. Furthermore, real-time reaction monitoring using spectroscopic techniques, such as X-ray diffraction (XRD) and Raman spectroscopy, has provided valuable insights into reaction kinetics and mechanistic pathways.

The increasing adoption of mechanochemistry aligns with the principles of green chemistry, offering a sustainable alternative to solvent-intensive methodologies. Future research will focus on enhancing mechanistic understanding through computational modelling, scaling up mechanochemical processes for industrial application, and further optimizing reaction efficiency through hybrid mechanochemical techniques. Moreover, the development of mechanochemical reactors with greater control over reaction parameters, such as pressure and temperature, will enable more predictable and reproducible synthetic outcomes. As the field continues to expand, collaborations between chemists, material scientists, and engineers will play a key role in realizing the full potential of mechanochemistry in both research and industry.

## 1.12 Application of Derivatized Chitosan

### 1.12.1 Biomedical Applications

Chitosan`s biocompatibility, biodegradability, and antimicrobial properties have made it an attractive candidate for various biomedical applications. It is extensively studied as a wound dressing material, where its ability to form films and hydrogel, coupled

with its inherent antibacterial properties, can promote and reduce infection risks. Furthermore, chitosan-based scaffolds are being developed for tissue engineering, where their porous structures facilitate cell adhesion, proliferation, and differentiation. The polycationic nature of chitosan also makes it suitable for drug and gene delivery systems; it can form nanoparticles or microspheres that encapsulate a therapeutic agent, thereby enhancing their stability and controlled release*[28]*.

### 1.12.2 Pharmaceutical and Nutraceutical Uses

Beyond its role in direct medical applications, chitosan is being studied for its potential in pharmaceutical formulations as an excipient. Its mucoadhesive properties extend the retention time of drugs in the gastrointestinal system, thereby improving their bioavailability. Furthermore, modified chitosan derivatives have shown promise as targeted drug carriers for cancer treatments, allowing precise delivery to affected cells. In the nutraceutical sector, its ability to bind fats has led to the development of dietary supplements designed to help regulate cholesterol levels, further demonstrating its health benefits*[29]*.

### 1.12.3 Environmental and Industrial Applications

The unique chemical and physical properties of chitosan make it valuable in environmental and industrial sectors as well. Due to its cationic nature, it serves as an effective flocculant in wastewater treatment, aiding in the removal of heavy metals and dyes. Additionally, chitosan-based biodegradable films and coatings are being investigated as sustainable alternatives to conventional plastic packaging. In agriculture, it functions as a natural biopesticide and plant growth enhancer, as research indicates that it can activate the plant's innate defense mechanisms against environmental stress and pathogens*[30]*.

### 1.12.4 Emerging Applications and Advanced Composites

Recent innovations have extended the use of chitosan into cutting-edge fields such as sensor technology and energy storage. By integrating chitosan with metal oxides like zirconium dioxide, researchers have developed advanced composite materials with superior mechanical and electrical properties. These versatile composites are being

explored for use in biosensors, catalytic, and flexible electronic devices. Additionally, the ability to chemically modify chitosan allows scientists to fine-tune its properties for specific applications, opening new possibilities for interdisciplinary research and technological advancements.

### 1.13 Purpose of the Study

The present study aims to develop a novel composite material through the mechanochemical grafting of acrylic acid onto chitosan (AA-g-CTS). This modification is designed to enhance the physicochemical properties of chitosan, such as its thermal stability, adsorption capacity, and surface reactivity. Using mechanochemistry provides a sustainable, solvent-free approach that aligns with green chemistry principles. The resulting material holds potential for application in environmental remediation, catalysis, and biomedical fields.

### 1.14 Hexavalent Chromium (Cr (VI)) as an environmental pollutant

Hexavalent chromium Cr (VI) is an extremely harmful and environmentally persistent heavy metal that often enters water through various industrial activities such as electroplating, textile dyeing, leather tanning, and metal finishing. Its presence in wastewater raises significant environmental concerns due to its high water solubility and strong oxidative potential, which enable it readily engage with biological systems *[31]*.

Compared to its trivalent form $Cr^{+3}$, $Cr^{+6}$ is substantially more dangerous, largely because it can penetrate cell membranes and trigger mutagenic and carcinogenic effects. Consequently, it is categorized as a priority pollutant by numerous environmental regulatory bodies. The pollution of aquatic environments by $Cr^{+6}$ not only disrupts ecological equilibrium but also poses server health risks to humans through exposure via drinking water and the food chain *[32]*.

Various treatment technologies have been developed to eliminate Cr+6 from wastewater. These approaches typically fall into categories that include chemical reduction precipitation, coagulation, membrane separation, and adsorption[1,3,4]. Among them, adsorption is widely viewed as an effective and environmentally friendly method due to its straightforward operation and adaptability to diverse water treatment situations*[32]*.

Recent studies have concentration on creating cost effective, biodegradable, and high-performance adsorbents made from natural materials and nanostructured system. These material present significant potential for removing $Cr^{+6}$ ions through surface interactions and coordination with function groups [33],[32].

In this regard, the present study explores the viability of acrylic acid -grafted chitosan as an adsorbent for the removal of $Cr^{+6}$ from aqueous solution. The grafting process introduces more functional group to chitosan, increasing the material's capacity to bind with heavy metal ions, making it a promising option for sustainable water treatment solutions.

# CHAPTER 2

# MATERIALS AND METHODS

This chapter outlines the material, reagents, and experimental methods used in the synthesis of acrylic acid grafted chitosan (AA-g-CTS). The work focuses on modifying chitosan, a natural biopolymer, to enhance its functional properties through grafting and inorganic nanoparticle incorporation.

This Material was produced using a mechanochemical approach, an energy-efficient method that minimizes the use of solvent and allows for solid-state reaction through grinding or milling. This environmentally friendly synthesis technique facilitates the creation of advanced functional materials with potential uses in water treatment, catalysis, and biomedical applications.

## 2.1 Chemicals used

Table No. 2.1 Chemicals used

| Chemicals | Company | Purity |
|---|---|---|
| Chitosan | Sigma Aldrich | 99 % |
| Acrylic acid | Sigma Aldrich | 99 % |
| $K_2Cr_2O_7$ | Qualigens | 99.5 % |
| $K_2S_2O_8$ | Fisher Scientific | 99 % |
| Acetic Acid | Merck Millipore | 100 % |
| Ceric ammonium nitrate (CAN) | Sigma Aldrich | 98.5% |
| NaOH | SRL | 98 % |
| HCl | Avra | |

## 2.2 Preparation of Acrylic acid grafted Chitosan (AA-g-CTS) by Conventional method

A method previously reported was adapted and modified to graft acrylic acid onto chitosan. To start, a 1% (w/v) solution of chitosan was prepared. Next, 0.1 M ceric ammonium nitrate (CAN), which was dissolved in 1N nitric acid, was gradually added as an initiator. Following this, a 2% acrylic acid solution (in distilled water) was slowly

incorporated into the mixture while maintaining continuous stirring and under UV radiation exposure. The grafting process was conducted at a temperature of 70 °C for a duration of 45 minutes. Upon completion of the reaction, sodium hydroxide (NaOH) was used to treat the mixture, resulting in the precipitation of the grafted product. The solid obtained was then washed thoroughly with distilled water many times to remove any unreacted monomers and impurities. Finally, the purified product was dried in an oven at a temperature range of 50–55 °C.

### 2.3 Preparation of Acrylic acid grafted Chitosan (AA-g-CTS) by mechanochemical method

Acrylic acid grafted chitosan (AA-g-CTS) was prepared via a mechanochemical method using potassium persulfate ($K_2S_2O_8$) as the initiator. Initially, 0.7 g of chitosan was placed in a mortar and pestle. To this, 0.3 g of potassium persulfate was added, and the mixture was ground continuously for 2 hours to ensure uniform dispersion and initiation of the radical reaction. Subsequently, 0.34 g of acrylic acid was added dropwise to the mixture while grinding was continued for an additional 3 hours. Upon completion, the product was thoroughly washed with distilled water to remove any unreacted monomers or by-products, followed by rinsing with 2% acetic acid to remove unreacted chitosan. The final material was dried in a hot air oven at 100 °C to obtain the grafting chitosan in powdered form.

### 2.4 Grafting Efficiency (%) and Percent (%) grafting

2.6.1 Grafting Efficiency (%)

Grafting Efficiency (GE) indicates the effectiveness of a monomer's attachment to a polymer backbone during the grafting process. This measurement is typically represented as a percentage and is defined as

$$\% \text{ Grafting Efficiency} = ( W_1 - W_o / W_2 ) \times 100$$

Where,

$W_1$= weight of grafted copolymer.

$W_o$=Weight of polymer taken.

$W_2$ =Weight of monomer taken.

2.6.2 Percent Grafting (%G)

The percent grafting serves as a quantitative indicator of the weight increase of a base polymer resulting from the successful grafting of monomer chains onto its backbone. It shows the proportion of grafted material that has been added in comparison to the original weight of the polymer. This metric is crucial for assessing the degree of modification achieved during graft copolymerization processes.

% Grafting (%G) = $[(W_1 - W_o) / W_o] \times 100$

Where,

W1 weight of grafted copolymer

Wo = Weight of polymer taken.

**2.5 Procedure for pHpzc Analysis:**

The salt addition technique was performed by adding identical amounts of the substrate to a set of solutions of the same ionic strength at different pH values (Anderson and Rubin 1981; Tan et al. 2008; Mahmood et al. 2011). In a series of 50-mL centrifuge tubes, 0.2 g of sample was added to 40.0 mL of 0.1 M NaNO3 solution. The pH was adjusted with 0.1 M HNO3 and 0.1 M NaOH as needed, to obtain the appropriate pH range of 2, 3, 4, 5, 6, 7, 8, 9, 10, and 11 (± 0.1 pH units). The pH values of the supernatant in each tube were denoted as pHi. The samples were shaken for 24 h using a rotary agitator (Wrist-Action Shaker, Cole Parmer 51704 Series) at 200 rpm. After settling, the pH values of the supernatant in each tube were measured and denoted as pHf. The PZC was obtained from the plot of ΔpH (=pHf – pHi) against pHi. Experiments were repeated with a 0.05 M NaNO3 solution. Each set of experiments was performed in triplicate and the mean value was recorded. Samples of natural kaolinite and synthetic goethite were also analyzed by the above procedure for comparison with previously published values.

**2.6 Establishing Calibration for Potassium Dichromate ($K_2Cr_2O_7$)**

Creating Calibration for Potassium Dichromate ($K_2Cr_2O_7$) Solutions To measure the concentration of $Cr^{6+}$ ions in the solution, a calibration curve was developed using standard potassium dichromate ($K_2Cr_2O_7$) solutions. A primary stock solution was prepared by dissolving a precisely measured quantity of $K_2Cr_2O_7$ in deionized water.

From this stock solution, a series of standard solutions with concentrations of 5, 10, 15, 20, and 25 ppm were generated through a process of serial dilution. The absorbance for each standard solution was measured using a UV-Visible spectrophotometer at a wavelength corresponding to the peak absorbance of Cr (VI) (typically around 360 nm), with deionized water serving as the blank. A graph was created to plot absorbance versus concentration to construct the calibration curve. This calibration curve was then used to determine the concentrations of Cr (VI) in unknown samples during the adsorption studies.

### 2.7 Optimization of adsorption parameter

To assess the adsorption characteristics of Cr (VI), a series of batch test were performed by altering important parameter such as pH ( from 3 to 10 ), time duration (from 60 minutes to 240 minutes ), initial chromium concentration (between 80 ppm to 140 ppm), and the amount of material utilized (from 0.1 g to 0.3 g ) at 298 k temperature. In each experiment , a specific quantity of the composite material was introduced into a chromium solution with a known concentration.

The solution was stirred for a designated period, then filtered to separate the adsorbent. A sample of the clear filtrate was analyzed using a UV-spectrophotometer at 360 nm to determine the remaining concentration of Cr (VI).

$$q_e = (C_0 - C) \cdot V / m$$

The composite's adsorption capacity (qe) was calculated using the following formula. I In this context, qe represents the adsorption capacity (mg/g); Co and C denote the initial and equilibrium concentrations of Cr (VI) (mg/L); V indicates the volume of the solution (L); and m refers to the mass of adsorbent (g) *[34]*.

### 2.8 Adsorption Isotherms

Adsorption isotherm illustrates the connection between the quantity of adsorbate that adheres to the surface of the adsorbent and its concentration in the solution at a consistent temperature. These models assist in comprehending the characteristics of the surface and the interaction mechanisms that play a role in the adsorption process. Numerous isotherms and kinetic models are typically utilized to evaluate adsorption data.

**Langmuir Isotherms**:

The Langmuir model posits that adsorption occurs in a monolayer on a uniform surface that has a limited number of identical sites. It indicates that after a site is filled, no additional adsorption can happen at that specific site. The model is formulated as follows.

$$\frac{c_e}{q_e} = \frac{1}{k_L qmax} + \frac{c_e}{qmax}$$

Where Ce denotes the equilibrium concentration (mg/L), $q_e$ represents the amount adsorbed at equilibrium (mg/g), $q_{max}$ signifies the maximum adsorption capacity (mg/g), and $K_L$ refers to the Langmuir constant associated with the affinity of the binding sites*[35]*.

**Freundlich Isotherm**

The Freundlich model characterizes adsorption on surfaces that are not uniform and presumes that multilayer adsorption occurs. This model is empirical and can be represented by the following equation:

$$log\ q_e = log\ K_F + \frac{1}{n} \log Ce$$

In this equation, $K_F$ (mg/g) $(L/mg)^{1/n}$ and n are the Freundlich constants that pertain to the capacity and intensity of adsorption, respectively*[35]*.

**Temkin Isotherm**

The Temkin model posits that as the surface coverage increases, the heat of adsorption decreases in a linear fashion because of the interactions between the adsorbate and the adsorbent. The linear representation of the Temkin equation is:

$$q_e = B \ln A + B \ln C_e$$

Where A(L/g) represents the equilibrium binding constant of the Temkin isotherm, B is defined as b divided by the product of the gas constant R and the absolute temperature T, where R is the gas constant (8.314 J/mol K), T is the absolute temperature in kelvine and b is associated with the heat of adsorption*[36]*.

## 2.9 Instrumentation

**FT-IR**

Fourier Transform Infrared Spectroscopy (FTIR) is a key analytical method for examining molecular structures by detecting the vibrations of chemical bonds. It provides a unique spectral pattern for different compounds, allowing for the identification of functional groups and verification of structural modifications. By recording the absorption of infrared radiation at specific wavelengths, FTIR generates spectra that reflect chemical changes. In grafting research, the presence of a new absorption band or shifts in existing peaks confirms successful functionalization. This non-destructive technique is widely applied in polymer science and biomaterials development, and chemical analysis.

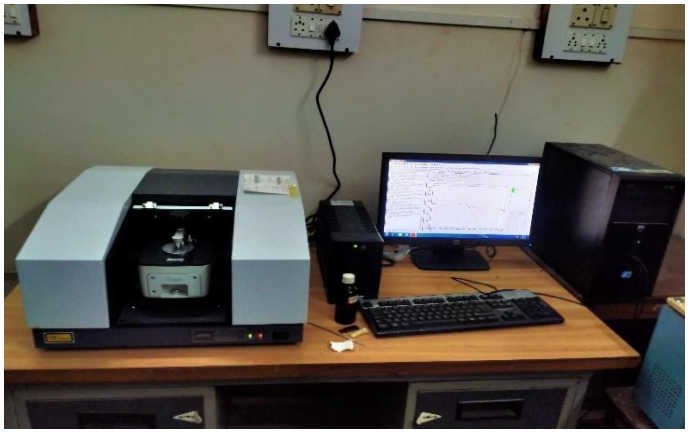

**Fig 2.1 FTIR Instrument**

## XRD

X-ray diffraction (XRD) is an essential technique for examining the crystalline nature of materials by analyzing the diffraction patterns of X-rays. It offers insights into the phase composition, crystallite size, and structural characteristics. When X-rays interact with a crystalline substance, they generate a distinct diffraction pattern determined by the atomic arrangement. In grafting studies, XRD is used to assess changes in crystallinity, confirming successful modification. This non-destructive method plays a crucial role in materials science, polymer research, and nanotechnology for structural evaluation.

**Fig 2.2 Powder X-ray Diffractometer**

## UV

The UV-Vis spectrophotometer operates on the principle of light absorption in the ultraviolet or visible spectrum by molecules that have π-electrons or non-bonding electrons. This absorption leads to the excitation of electrons to higher anti-bonding molecular orbitals. When the energy difference between the highest occupied molecular orbital (HOMO) and the lowest unoccupied molecular orbital (LUMO) is minimal, electron excitation is more likely to occur. UV-Vis spectroscopy quantifies the amount of light that passes through a sample (I) compared to the intensity of the incoming light (Io). This transmission is usually represented as a percentage ratio (I/Io) referred to as %T. The absorbance (A) is determined using the following formula:

$$A = - \log (\%T/100)$$

For this research, the UV-2600 UV-Vis spectrophotometer manufactured by Shimadzu (Japan) was utilized to analyze the concentration of various analytes. The instrument's functionality and its relevance to the current study are outlined below.

## BET and BJH Analysis

The BET method is commonly employed to determine the specific surface area of porous substances by assessing nitrogen gas adsorption at liquid nitrogen temperature. It relies on

the multilayer adsorption theory and yields insights into the accessible surface area. In conjunction with this, the BJH method analyzes the pore size distribution and pore volume through thse desorption branch of the isotherm. These techniques are crucial for characterizing the surface structure and porosity of materials, which affect their effectiveness in a range of applications.

# CHAPTER 3

# RESULT AND DISCUSSION

## Result and discussion

### 3.1 Calculation of Grafting Efficiency (GE) and Percent Grafting (%G)

Table No. 3.1 Grafting Efficiency and Percent Grafting

| Sr | Method | Grafting Efficiency (%) | Percent Grafting (%) |
|---|---|---|---|
| 1 | Conventional | 72 % | 34.97 % |
| 2 | Mechanochemical | 123.52 % | 60 % |

The grafting efficiency and % grafting of AA-g-CTS were found to be higher than the prepared by conventional method. This suggests that the mechanochemical method if more efficient for synthesis of chitosan derivative compare to reported conventional methods. The prepared AA-g-CTS was further characterized by FTIR and XRD.

### 3.2 Characterization of Acrylic Acid-Grafted Chitosan (AA-g-CTS)

#### 3.2.1 FT-IR

In order to detect the functional groups, present in the prepared material FTIR analysis of different compounds has been recorded. To identify the changes occurred in CTS after grafting, FTIR spectra of chitosan, acrylic acid and acrylic acid grafted chitosan was recorded and the corresponding results are shown in **Fig.3.1(a-d). Fig.3.1a** shows FTIR spectra of CTS, a strong band in the region of 3291-3361 $cm^{-1}$ is attributed to O-H and N-H stretching whereas, absorption band at 2928 and 2869 $cm^{-1}$ indicates asymmetric and symmetric C-H stretching respectively. Absorption band at 1655 $cm^{-1}$ indicates C=O stretching (amide I) whereas N-H bending is observed at 1576 $cm^{-1}$ (amide II) and C-N stretching at 1319 $cm^{-1}$. The peak at 1418 $cm^{-1}$ and 1371 $cm^{-1}$ indicates $CH_2$ bending and $CH_3$ symmetrical deformation. Furthermore, Absorption band for C-O-C asymmetric stretching is observed at 1154 $cm^{-1}$ *[37]*. Whereas, C-O stretching band is observed at 1058 and 1027 $cm^{-1}$. The signal at 895 $cm^{-1}$ corresponds to the presence of out of plane CH bending for monosaccharides. Furthermore, **Fig.3.1b** shows FTIR spectra of AA, a broad band in the region of 2400-3400 $cm^{-1}$ corresponds to the presence of O-H stretching of -COOH group, furthermore, due to $\alpha$ - $\beta$ unsaturation, characteristic peak of C=O is observed at lower frequency region at 1694 $cm^{-1}$,whereasas, peak at 981 $cm^{-1}$ and

corresponds to the presence of H-C=C, peak in the range of 1640-1650 $cm^{-1}$ corresponds to the presence of C=C double bond. **Fig.3.1c** shows FTIR spectra of AA-g-CTS prepared by conventional method as reported by S.F. Hamza *et al*. whereas, **Fig.3.1d** shows the FTIR spectra of AA-g-CTS prepared by solvent free mechanochemical method. **Fig.3.1d** shows a broad band in the range of 2400 3400 $cm^{-1}$ which suggests the existence of that -COOH group of AA, however, absorption band of C=O is shifted to higher frequency region of 1721 $cm^{-1}$ which suggests that C=C bond is get converted into C-C bond. Furthermore, peak at 981 $cm^{-1}$ and 810 $cm^{-1}$ corresponding to H-C=C is absent in AA-g-CTS which suggests that AA is linked with chitosan through ether linkage rather than amide linkage *[38]*. the existence of  This can be again confirmed by existence of amide (I, II and III) peaks in AA-g-CTS. The FTIR spectra of mechanochemically prepared AA-g-CTS resembles well with those prepared by reported conventional method which suggest that present method is suitable to derivatize CTS even in the absence of any solvent and harsh reaction conditions. To observe the phase change XRD analysis were performed.

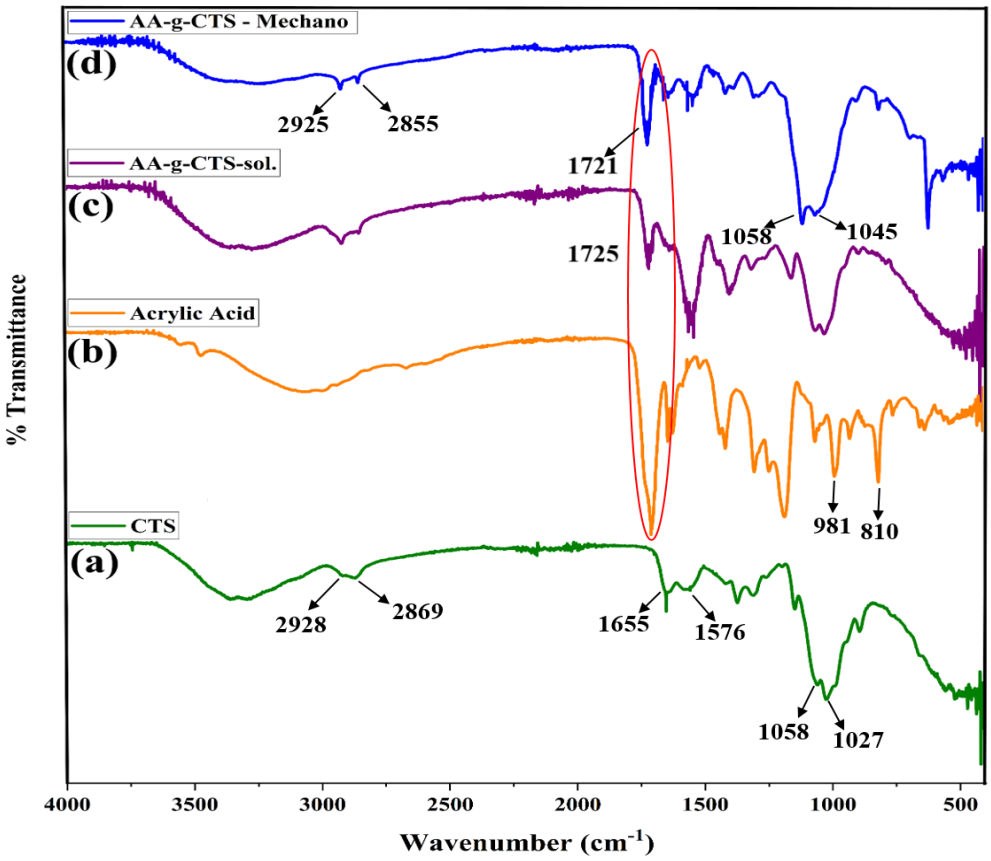


**Figure 3.1 FTIR spectra of (a) CTS (b) acrylic acid (c) AA-g-CTS solution method (d) AA-g-CTS mechanochemical method.**

### 3.2.2 XRD

As seen in Figure 3.2 X-ray diffraction (XRD) was performed to observe the change in the crystallinity of chitosan before and after grafting with acrylic acid. The XRD pattern of chitosan exhibits two distinct diffraction peaks at 9.65° and 19.96°, which correspond to its hydrated crystalline structure. These peaks indicate the semicrystalline nature of chitosan, resulting from the organized arrangement of polymer chains.

In contrast, the XRD pattern of acrylic acid-grafted chitosan (AA-g-CTS) exhibits a broad and less intense diffraction pattern, lacking distinct peaks. This suggests a reduction in crystallinity after grafting, likely due to the disruption of intermolecular hydrogen bonding within chitosan. The decreased crystallinity indicates successful grafting, as the introduction of acrylic acid reduces the polymer's ordered structure, making it more amorphous*[38]*.

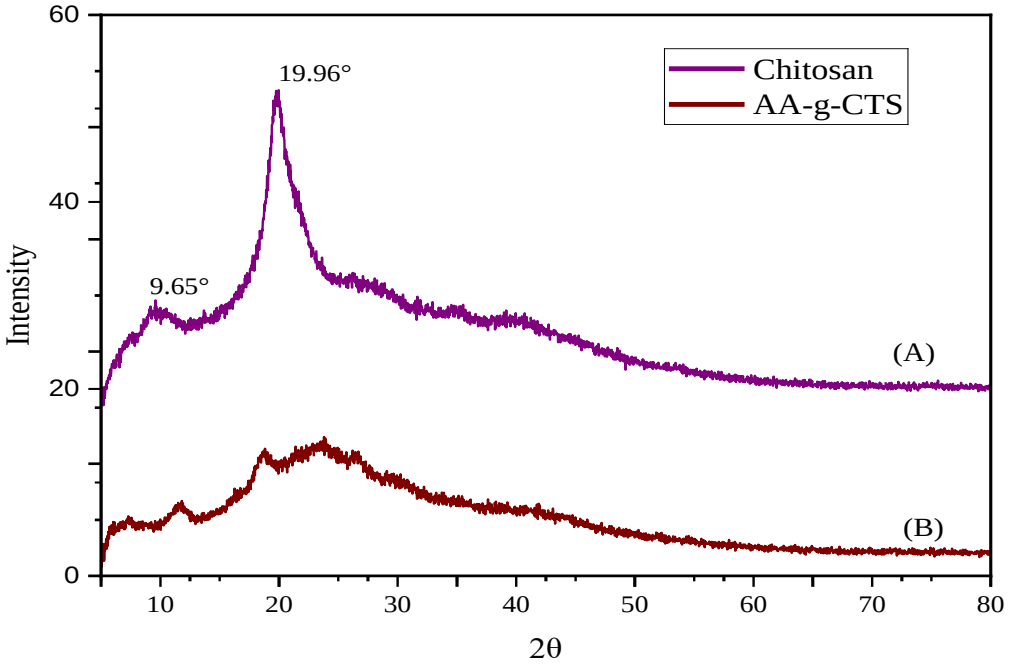


**Fig. 3.2 Shows XRD – Pattern of (A) Chitosan and (B) Acrylic acid grafted chitosan (AA-g-CTS).**

### 3.2.3 BET

The textural properties of the synthesized AA-g-CTS were examined using the Brunauer–Emmett–Teller (BET) technique, and the pore size distribution was assessed using the Barrett–Joyner–Halenda (BJH) model. The nitrogen adsorption–desorption isotherm of AA-g-CTS, according to the IUPAC classification, displayed a Type IV isotherm with an H3-type hysteresis loop, indicating the existence of mesoporous structures characterized by slit-like pores. *[39]* [Fig. 3.3 (a)].

The BET surface area measured for AA-g-CTS was 8.147 $m^2/g$, whereas, the BJH pore size distribution graph, illustrated in Fig. 3.3 (b), showed a varied pore structure with a predominant pore radius of about 1.87 nm and a total pore volume of 0.0157 cc/g, further confirming the material's mesoporous nature. The mesoporous nature of material enhance the adsorption of substrate molecules by providing more active sites. Thus, on the basis of FTIR, XRD and BET analysis it was interpreted that the AA-g-CTS was prepared successfully by mechanochemical approach, which can be used as an adsorbent for heavy metal removal and water remediation.

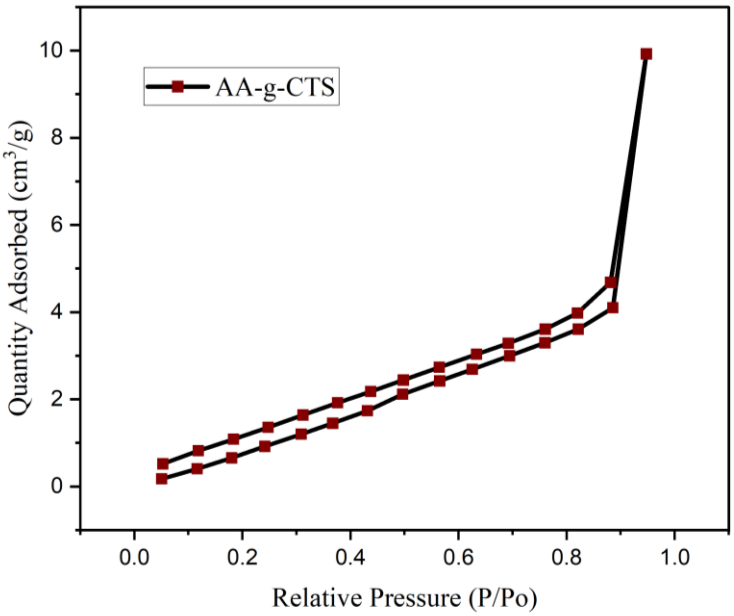


**(a)**

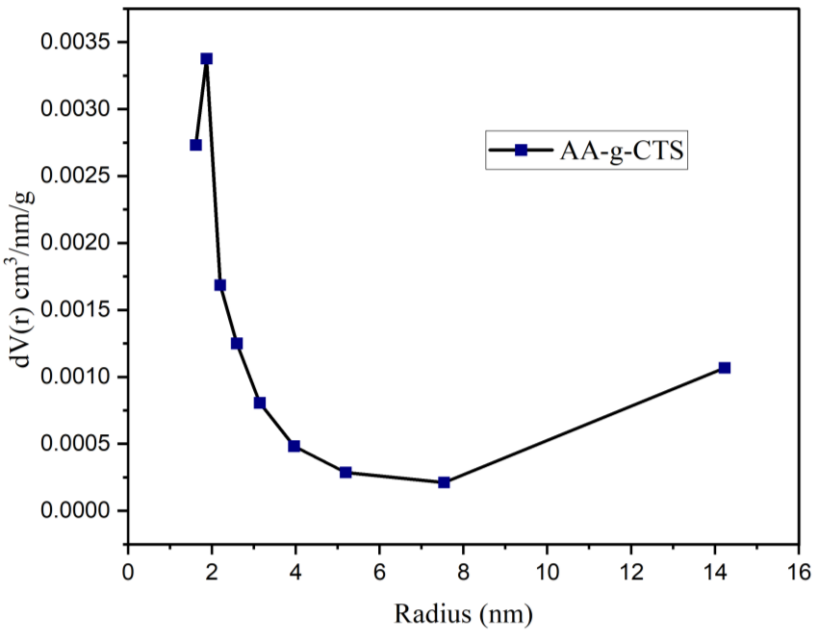


**(b)**

**Fig. 3.3 (a) BET analysis of AA-g-CTS (b) BJH analysis of AA-g-CTS**

Table No. 3.2 Data of BET and BJH

| **Surface Are ($m^2/g$)** | **Pore Volume ($cm^3/g$)** | **Average Pore Size (nm)** |
|---|---|---|
| 8.147 | 0.0157 | 1.869 |

### 3.3 Zeta Potential

Zeta potential analysis is done for analysis of surface charge of material (Adsorbent). The instrument used for analysis of zeta potential was Nano Book Omni 90 Plus instrument and results are presented in the form millivolt (mV). Fig.3.4 displayed the zeta potentential graph obtained by plotting zeta potential (mV) Vs various pH. The zeta potential value of AA-g-CTS was found to be 8.1 mV with calculated Isoelectric potential value 6.2. Surface charge behaviour was further confirmed by Point of Zero Charge (pHzpc) analysis.

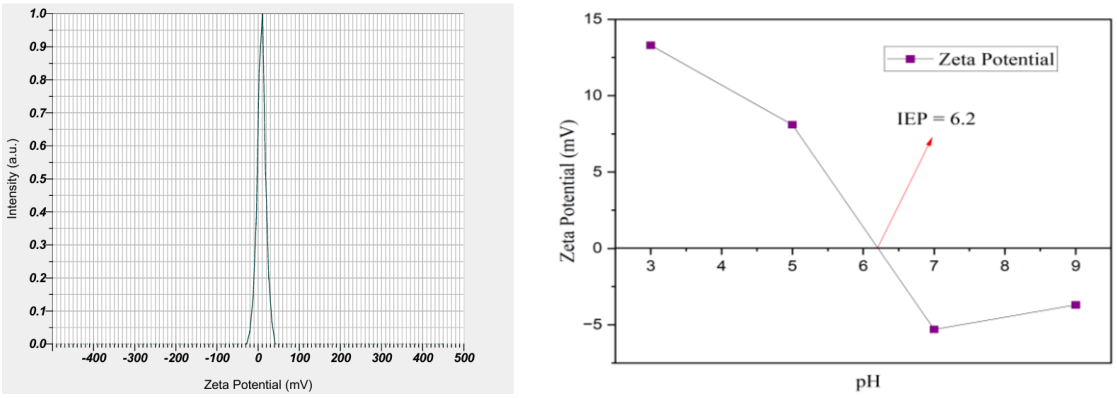


a b

**Fig. 3.4 Show( a) Zetapotential (b) Zetapotential Vs pH**

### 3.4 Point of Zero Charge (pHzpc)

The seen in Figure 3.5 the pHpzc of AA-g-CTS is 3.08.The point of zero charge (pHzpc) plays a critical role in the adsorption process. When the pH of the solution is above the pHzpc of the adsorbent (acrylic acid grafted chitosan), the surface acquires a net negative charge. In the present study, the pHzpc of acrylic acid grafted chitosan was found to be 3.08, while the optimized adsorption pH was 5, indicating that the material possesses a negatively charged surface under these conditions. Analyte chromate ions ($CrO_4^{2-}$), with a pKa of approximately 6.5 for the $HCrO_4^- \rightleftharpoons CrO_4^{2-}$ equilibrium, exist predominantly in the $HCrO_4^-$ form at pH 5. Although both $HCrO_4^-$ and $CrO_4^{2-}$ are negatively charged, the lower valence (–1) of $HCrO_4^-$ facilitates electrostatic interaction with the positively charged amine groups on chitosan derivatives at slightly acidic pH, enhancing the adsorption efficiency.

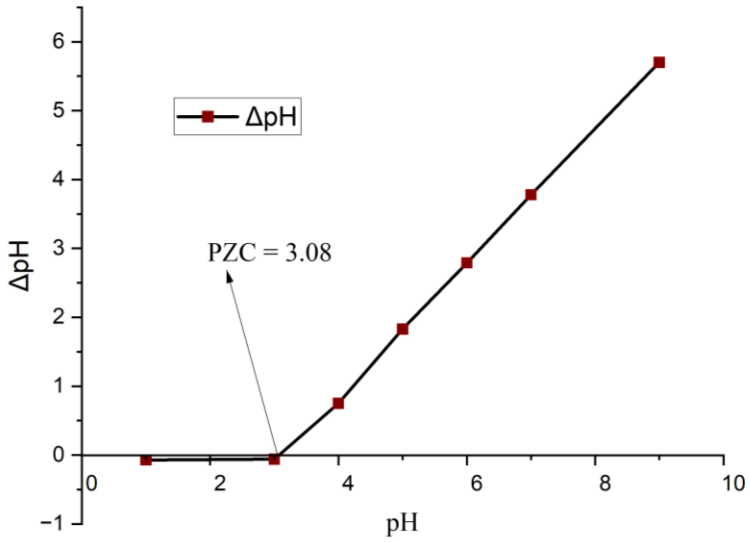


**Fig. 3.5 Point of zero charge of AA-g-CTS**

### 3.5 Calibration curve of $K_2Cr_2O_7$

To estimate the concentration of potassium dichromate a standard calibration curve has been prepared, and the instrument used is the UV-vis spectrophotometer. Without the calibration curve, the concentration of potassium dichromate can't be determined.

So, the of standard potassium dichromate is nm (from Fig. 3.6). That wavelength will be used to identify the absorption that needs to be considered to calculate the concentration of potassium dichromate in extracts in later research work.

The slope of the calibration graph of standard potassium dichromate will give the molar extinction coefficient value. So, the molar extinction coefficient for potassium dichromate is 0.0306 L/mol cm (from Fig. 3.7). This value will be used to calculate the concentration of potassium dichromate using Lambert-Beer's law.

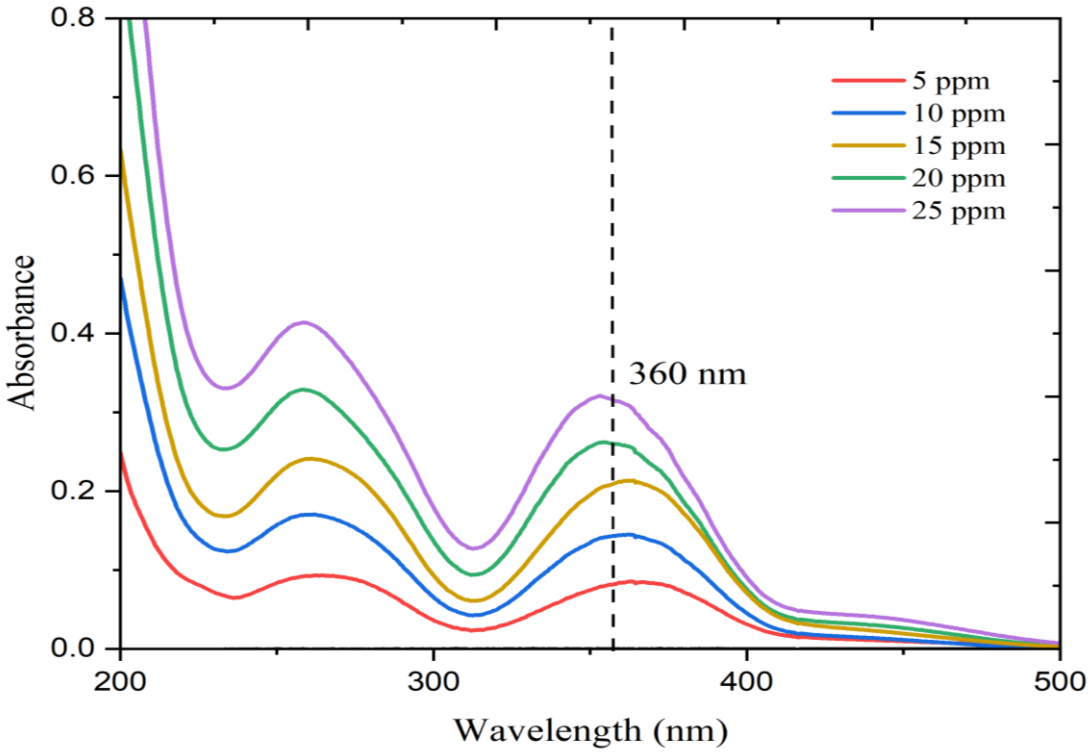


**Fig 3.6 – UV data of standard Potassium dichromate ($K_2Cr_2O_7$)**

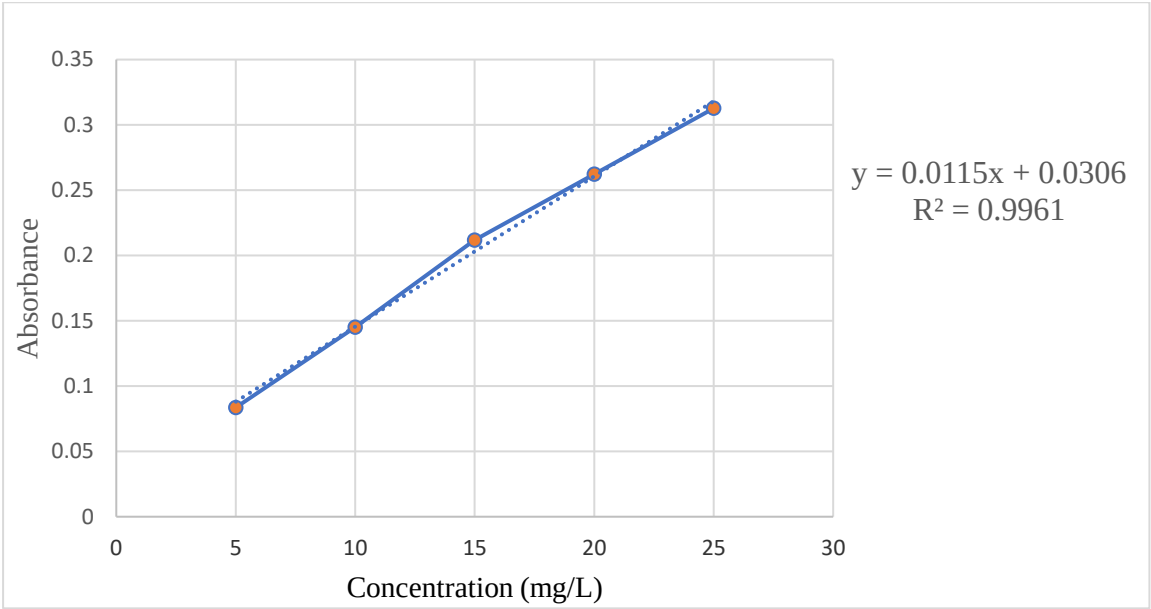


**Fig 3.7- Calibration graph of standard Potassium dichromate ($K_2Cr_2O_7$)**

Lamberts beers law- Concentration can be calculated by using lamberts beers

law i.e. The energy absorbed or transmitted by a solution depends on both the molar absorptivity of the solution and the concentration of the solute, that are proportional to each other.

$$\mathbf{A = \varepsilon cl}$$

Where

A=absorbance

ε = molar extinction coefficient ($LMol^{-1}$ $cm^{-1}$)

c= concentration

l = path length

### 3.6 Adsorption Properties

#### 3.6.1.. Effect of dose

The influence of adsorbent mass on the adsorption of [metal ion, e.g., Cr (VI)] onto the synthesized adsorbent was investigated at 298 K using an initial concentration of th6 metal ion at 100 $mg \cdot L^{-1}$. The mass of the adsorbent was varied between 100 and 300 mg, with the outcomes illustrated in Figure 3.8. indicating that a greater number of adsorption sites became accessible. However, the % binding diminished as the amount of adsorbent increased, likely due to the possible overlap or aggregation of adsorption sites, resulting in a reduced surface area available for adsorption per unit mass.

This pattern aligns with the established behavior observed in adsorption systems, where enhancing the adsorbent dose increases overall removal while reducing the specific adsorption capacity. At higher dosages, the removal efficiency reached a plateau, indicating that a saturation threshold was being met, where most of the available metal ions had been effectively adsorbed.

These findings imply that the ideal adsorbent dosage falls within the lower to mid-range of values tested, optimizing both high removal efficiency and effective use of the adsorbent.

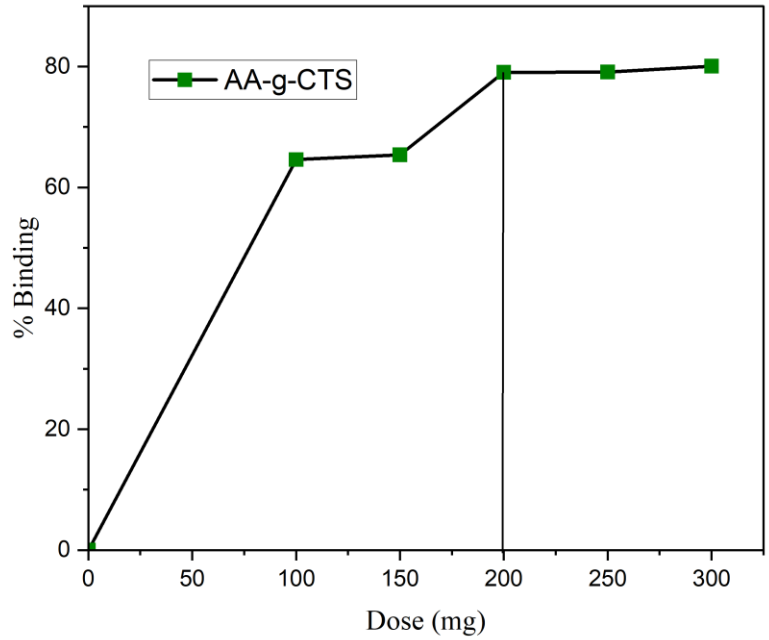


**Fig. 3.8 Impact of dose on the adsorption of Cr (VI) onto the AA-g-CTS (pH = 3, T = 298 K, Co = 100 mg/L, V = 50 mL, n = 200 rpm ).**

### 3.6.2. Effect of Time

The influence of contact time on the adsorption of Cr (VI) onto AA-g-CTS was examined at ambient temperature, and the findings are illustrated in Figure 3.9. The adsorption capacity (q) significantly increased during the initial phase, reaching around 18.3 mg/g within the first hour. This rapid adsorption is likely due to the high number of available active sites on the adsorbent's surface. As time went on, the rate of adsorption slowed and gradually approached equilibrium at approximately 180 minutes, where the observed maximum adsorption capacity was around 26.2 mg/g. This leveling off signifies that most of the active sites were filled and that the adsorption process became constrained by slower diffusion into the deeper pores. A minor decrease in adsorption capacity at 240 minutes may be linked to desorption or reorganization of Cr (VI) ions on the surface of the adsorbent. In general, the results indicate that 180 minutes is the optimal contact time for efficient Cr (VI) removal using AA-g-CTS at room temperature.

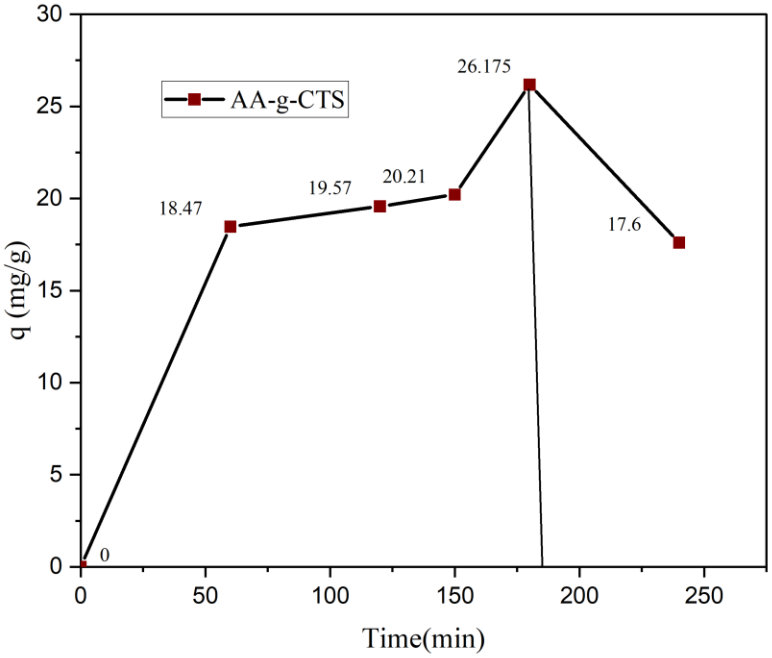


**Fig. 3.9. Impact of time on the adsorption of Cr (VI) onto the AA-g-CTS (pH = 5, T = 298 K, Co = 100 mg/L, V = 50 mL, mass = 0.200 g , n = 200 rpm ).**

### 3.6.3 Effect of pH

The influence of pH on Cr (VI) adsorption by AA-g-CTS was examined within a pH range of 3 to 10, as presented in Figure 3.10. The adsorption capacity increased from pH 3 to 5, achieving a peak of approximately 26.3 mg/g at pH 5. However, further increases in pH resulted in a decline in adsorption, with the minimum observed at pH 10. This pattern indicates that pH significantly impacts the adsorption process. The enhanced efficacy at lower pH levels is likely attributed to the surface of the adsorbent being negatively charged, which draws in the positively charged Cr (VI) ions.

This is corroborated by the point of zero charge (pHzpc) of AA-g-CTS, noted to be 3.08 (Figure 3.6). Above this pH level of 3.08, the adsorbent surface carries a negative charge, which improves the electrostatic attraction between the adsorbent and Cr (VI) cations. When the pH below 3.08, the surface shifts to a positive charge, causing repulsion that diminishes Cr (VI) adsorption. Additionally, the abundance of $OH^-$ ions at elevated pH levels may compete for the active sites, further reducing the adsorption capacity. Consequently, the optimal pH for Cr (VI) removal using AA-g-CTS occurs around pH 5.

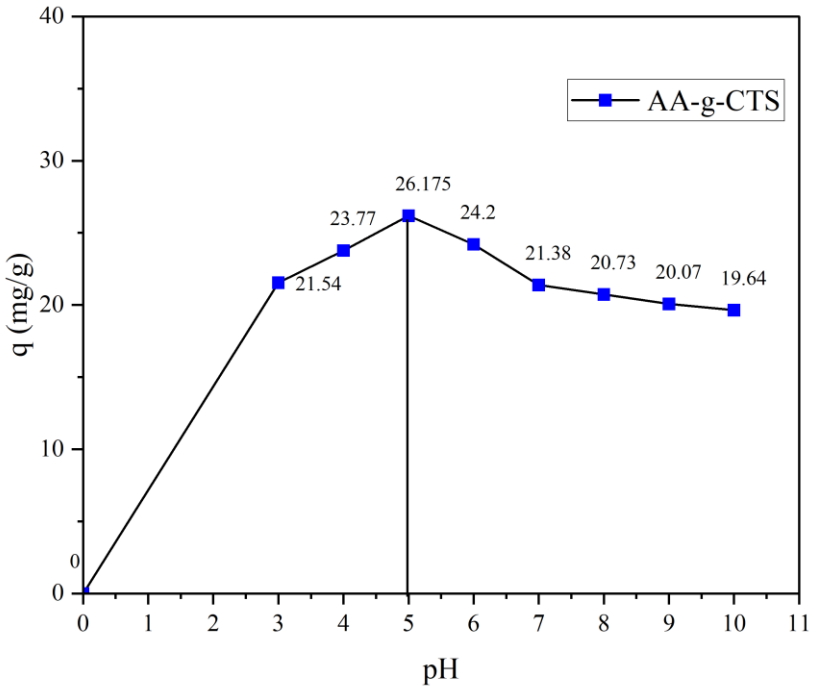


**Fig. 3.10.Impact of pH on the adsorption of Cr (VI) onto the AA-g-CTS (t= 180 min, T = 298 K, Co = 100 mg/L, V = 50 mL, mass = 0.200 g , n = 200 rpm ).**

### 3.6.4 Effect of Concentration

The effect of the initial concentration of Cr (VI) ions on the adsorption effectiveness of AA-g-CTS was examined by adjusting the metal ion concentration between 80 and 140 ppm. The obtained adsorption capacities (q, mg/g) are depicted in Figure 3.11 According to the graph, the adsorption capacity of AA-g-CTS notably rises from 14.5 mg/g at 80 ppm to 17.4 mg/g at 100 ppm, demonstrating the presence of plentiful active sites on the grafted polymer for Cr (VI) absorption at lower concentrations. A further increase to 120 ppm the adsorption capacity was almost similar (17.6 mg/g), indicating that the available binding sites are approaching saturation. At 140 ppm, a small decrease is observed, likely due to the saturation of adsorption sites and potential competition among the excess Cr (VI) ions for the limited active groups. This pattern indicates that AA-g-CTS shows a strong preference for Cr (VI) ions

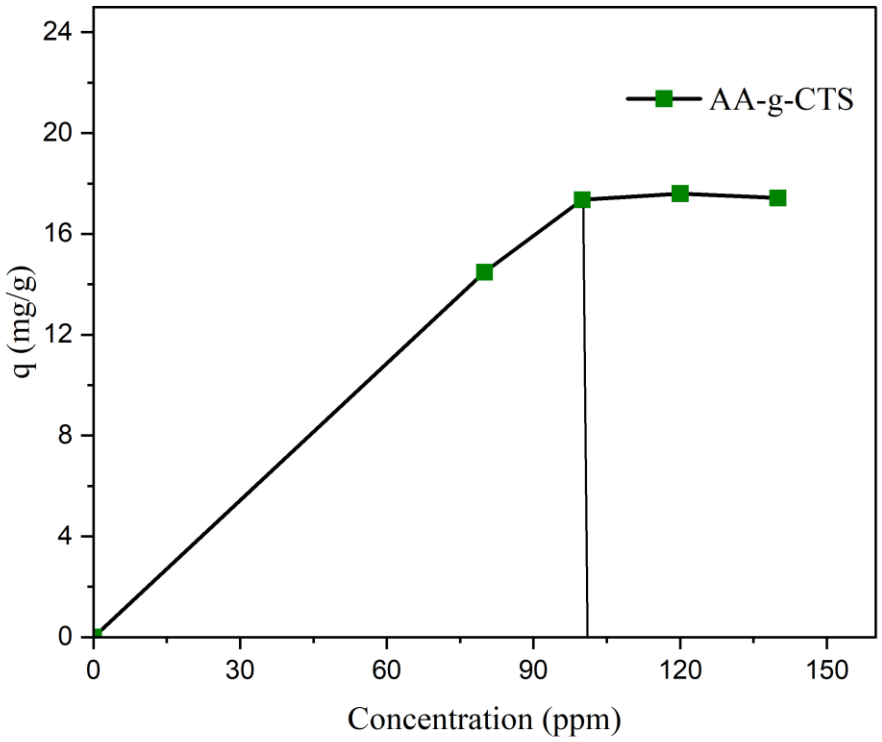


**Fig.3.11 Impact of concentration on the adsorption of Cr (VI) onto the AA-g-CTS (pH = 5, T = 298 K, V = 50 mL, n = 200 rpm )**

### 3.6 Adsorption Isotherm Models

To examine the adsorption characteristics of the selected adsorbent towards the targeted ion, three isotherms were applied: Langmuir, Freundlich, and Temkin. Each model was analyzed using its linear form, and the corresponding correlation coefficients ($R^2$), were used to compare the accuracy of fit to the experimental data.

#### Langmuir Isotherm

The Langmuir isotherm model shown in Figure 3.12, assumes adsorption occurs in a monolayer on a uniform surface, was represented by plotting Ce/qe versus Ce. The correlation coefficient ($R^2$= 0.940) demonstrated a good fit. By analysing the slope and intercept of the Langmuir plot. The maximum adsorption capacity (qmax) was found to be 43.29 mg $g^{-1}$, with a Langmuir constant ($K_L$) of 0.0238 L/mg

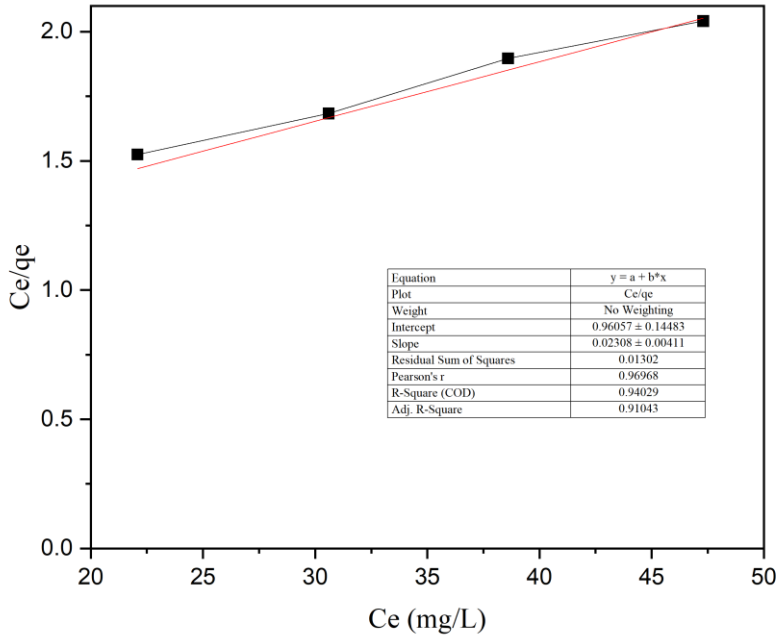


**Fig. 3.12 Langmuir isotherm**

Table No 3.3 Langmuir Data

| $q_{max}$ (mg/g) | $K_L$ L/mg | $R^2$ |
|---|---|---|
| 43.327 | 0.02407 | 0.94029 |

**Freundlich isotherm**

The Freundlich isotherm shown in Figure 3.13, considers multilayer adsorption on diverse surfaces, was evaluated using a log qe versus log Ce plot. This model demonstrated very high linearity ($R^2$= 0.9977), indicating multilayer adsorption property on AA-g-CTS. The Freundlich constant $K_F$ and 1/n were calculated to be 2.11 mg $g^{-1}$(L $mg^{-1}$) and 0.6208. respectively. The value of 1/n suggests that multilayered adsorption is favourable for AA-g-CTS. The value of n helps to identify whether the adsorption is physisorption (n > 1) or chemisorption (n<1)[41]. In the present work the n value found to be 1.617, which suggests

that the AA-g-CTS follows multilayered physisorption mechanism for adsorption of Cr (IV) ions [42].

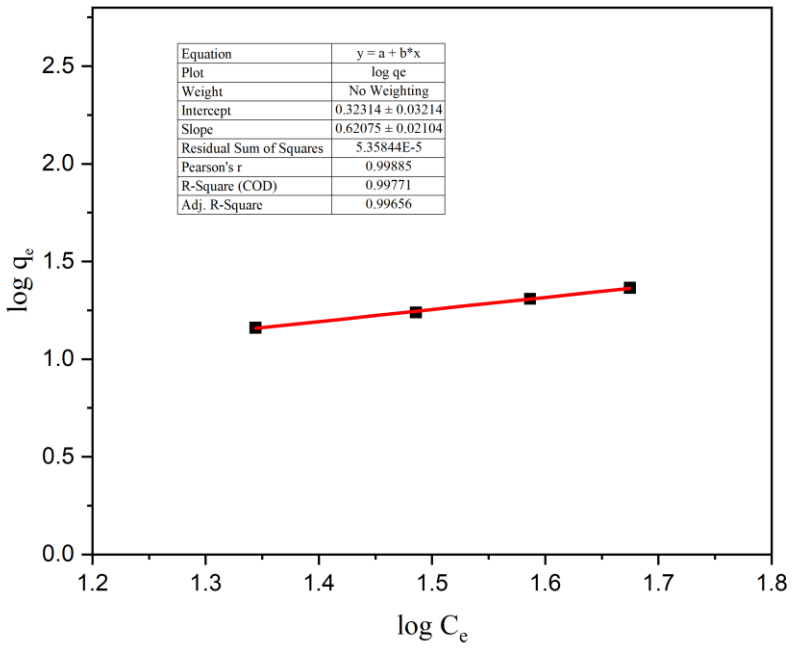


**Fig. 3.13 - shows the Freundlich isotherm**

Table No 3.4 Freundlich data

| **n** | **1/n** | **$R^2$** | **intercept** | **$K_F$ mg $g^{-1}$(L $mg^{-1}$)** |
|---|---|---|---|---|
| 1.617 | 0.618 | 0.9977 | 0.3282 | 2.129 |

**Temkin isotherm**

The Temkin isotherm model shown in Figure 3.14, accounts for the interaction between the adsorbate and adsorbent, was evaluated by plotting qe against ln Ce. With a correlation coefficient of $R^2$ = 0.9876, this model exhibited a good fit to the experimental data. The slope and intercept provided valuable information regarding the heat of adsorption and the Temkin binding constant. The value of B was found to be 11.409 mg/g, indicating a moderate adsorption capacity and suggesting a weak adsorbate and adsorbent interaction.

The bt value was 0.217 KJ/mol, which is less than 40 KJ/mol, confirming that the adsorption process follows physisorption rather than chemisorption [43].

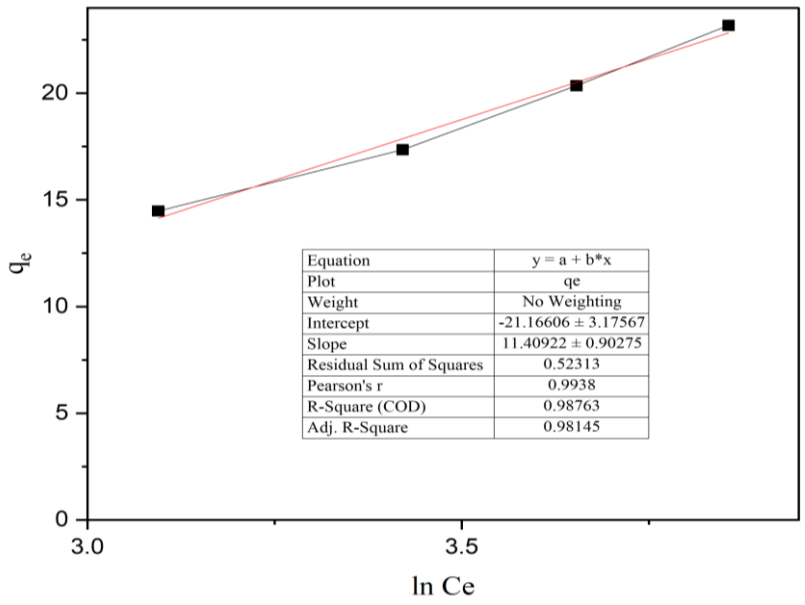


**Fig 3.14 shows the Temkin isotherm**

Table No 3.5 Temkin Data

| **A (1/g)** | **B mg/g** | **$R^2$** | **$b_t$ (KJ/mol)** |
|---|---|---|---|
| 0.156 | 11.409 | 0.987 | 0.217 |

# CHAPTER 4

# CONCLUSION

## 4.1 Conclusion

This research successfully synthesized acrylic acid-grafted chitosan (AA-g-CTS) using a mechanochemical approach that does not involve solvents, showcasing an environmentally friendly and effective method to improve the adsorption capability of chitosan for hexavalent chromium [Cr (VI)] ions. The occurrence of the grafting process was confirmed through FTIR analysis, which detected the acrylic acid functional groups on chitosan, and XRD analysis, which revealed a reduction in crystallinity, confirming the structural/phase alteration of the biopolymer. The calculated grafting percentage and grafting efficiency were 60% and 123.52%, respectively, reflecting the efficacy of the mechanochemical technique.

Surface characterization studies, such as zeta potential measurements and the determination of the point of zero charge (pHzpc), offered further understanding of the surface characteristics of the material. It was observed that the pHzpc of AA-g-CTS was 3.08, indicating that the surface carries a negative charge at optimized pH (pH = 5). This property facilitated greater adsorption of Cr (VI) specie under acidic conditions due to the electrostatic attraction between the positively charged Cr (VI) ions and the negatively charged surface of the adsorbent.

Batch adsorption tests demonstrated that AA-g-CTS reached a maximum adsorption capacity for Cr (VI) of 26.17 mg $g^{-1}$ under optimal conditions (pH 5, 0.2 g adsorbent, 100 ppm Cr (VI), 180 min contact time). Isotherm modelling supported the multilayered physisorption process

In summary, AA-g-CTS emerges as a promising, environmentally friendly, and highly effective adsorbent for the removal of Cr (VI). Future research should concentrate on the Kinetics, regeneration, and practical applications in real wastewater treatment systems.

# References


[1] J. Hou, B. E. Aydemir, and A. G. Dumanli, “Understanding the structural diversity of chitins as a versatile biomaterial,” Sep. 20, 2021, *Royal Society Publishing*. doi: 10.1098/rsta.2020.0331.

[2] I. Aranaz *et al.*, “Chitosan: An overview of its properties and applications,” Oct. 01, 2021, *MDPI*. doi: 10.3390/polym13193256.

[3] H. Amiri *et al.*, “Chitin and chitosan derived from crustacean waste valorization streams can support food systems and the UN Sustainable Development Goals,” *Nat Food*, vol. 3, no. 10, pp. 822–828, Oct. 2022, doi: 10.1038/s43016-022-00591-y.

[4] C. Casadidio, D. V. Peregrina, M. R. Gigliobianco, S. Deng, R. Censi, and P. Di Martino, “Chitin and chitosans: Characteristics, eco-friendly processes, and applications in cosmetic science,” 2019, *MDPI AG*. doi: 10.3390/md17060369.

[5] B. T. Iber, N. A. Kasan, D. Torsabo, and J. W. Omuwa, “A review of various sources of chitin and chitosan in nature,” 2022, *Tech Science Press*. doi: 10.32604/JRM.2022.018142.

[6] N. E. Mushi, “A review on native well-preserved chitin nanofibrils for materials of high mechanical performance,” May 01, 2021, *Elsevier B.V.* doi: 10.1016/j.ijbiomac.2021.02.149.

[7] M. K. Jang, B. G. Kong, Y. Il Jeong, C. H. Lee, and J. W. Nah, “Physicochemical characterization of α-chitin, β-chitin, and γ-chitin separated from natural resources,” *J Polym Sci A Polym Chem*, vol. 42, no. 14, pp. 3423–3432, Jul. 2004, doi: 10.1002/pola.20176.

[8] E. S. Abdou, K. S. A. Nagy, and M. Z. Elsabee, “Extraction and characterization of chitin and chitosan from local sources,” *Bioresour Technol*, vol. 99, no. 5, pp. 1359–1367, Mar. 2008, doi: 10.1016/j.biortech.2007.01.051.

[9] K. Mohan *et al.*, “Green and eco-friendly approaches for the extraction of chitin and chitosan: A review,” Jul. 01, 2022, *Elsevier Ltd*. doi: 10.1016/j.carbpol.2022.119349.

[10] N. A. Z. Abidin, F. Kormin, N. A. Z. Abidin, N. A. F. M. Anuar, and M. F. A. Bakar, “The potential of insects as alternative sources of chitin: An overview on the chemical method of extraction from various sources,” Jul. 02, 2020, *MDPI AG*. doi: 10.3390/ijms21144978.

[11] S. Kaur and G. S. Dhillon, “Recent trends in biological extraction of chitin from marine shell wastes: A review,” Mar. 01, 2015, *Informa Healthcare*. doi: 10.3109/07388551.2013.798256.

[12] I. Younes, O. Ghorbel-Bellaaj, R. Nasri, M. Chaabouni, M. Rinaudo, and M. Nasri, “Chitin and chitosan preparation from shrimp shells using optimized enzymatic deproteinization,” *Process Biochemistry*, vol. 47, no. 12, pp. 2032–2039, Dec. 2012, doi: 10.1016/j.procbio.2012.07.017.

[13] T. Sun, D. Zhou, J. Xie, and F. Mao, “Preparation of chitosan oligomers and their antioxidant activity,” *European Food Research and Technology*, vol. 225, no. 3–4, pp. 451–456, Jul. 2007, doi: 10.1007/s00217-006-0439-1.

[14] S. (Gabriel) Kou, L. M. Peters, and M. R. Mucalo, “Chitosan: A review of sources and preparation methods,” Feb. 01, 2021, *Elsevier B.V.* doi: 10.1016/j.ijbiomac.2020.12.005.

[15] D. Alemu, E. Getachew, and A. K. Mondal, “Study on the Physicochemical Properties of Chitosan and their Applications in the Biomedical Sector,” *Int J Polym Sci*, vol. 2023, pp. 1–13, Jul. 2023, doi: 10.1155/2023/5025341.

[16] C. Choi, J. P. Nam, and J. W. Nah, “Application of chitosan and chitosan derivatives as biomaterials,” Jan. 25, 2016, *Korean Society of Industrial Engineering Chemistry*. doi: 10.1016/j.jiec.2015.10.028.

[17] M. E. I. Badawy, “Structure and antimicrobial activity relationship of quaternary *N* -alkyl chitosan derivatives against some plant pathogens,” *J Appl Polym Sci*, vol. 117, no. 2, pp. 960–969, Jul. 2010, doi: 10.1002/app.31492.

[18] I. Aranaz, R. Harris, and A. Heras, “Chitosan Amphiphilic Derivatives. Chemistry and Applications,” 2010.

[19] J. ZHANG, Q. WANG, and A. WANG, “Synthesis and characterization of chitosan-g-poly(acrylic acid)/attapulgite superabsorbent composites,” *Carbohydr Polym*, vol. 68, no. 2, pp. 367–374, Mar. 2007, doi: 10.1016/j.carbpol.2006.11.018.

[20] W. Jones and M. D. Eddleston, “Introductory lecture: Mechanochemistry, a versatile synthesis strategy for new materials,” Dec. 01, 2014, *Royal Society of Chemistry*. doi: 10.1039/c4fd00162a.

[21] J. F. Ferná Ndez-Bertran, “Mechanochemistry: an overview*,” 1999.

[22] A. Krusenbaum, S. Grätz, G. T. Tigineh, L. Borchardt, and J. G. Kim, “The mechanochemical synthesis of polymers,” *Chem Soc Rev*, vol. 51, no. 7, pp. 2873–2905, 2022, doi: 10.1039/D1CS01093J.

[23] M. Solares-Briones *et al.*, “Mechanochemistry: A green approach in the preparation of pharmaceutical cocrystals,” *Pharmaceutics*, vol. 13, no. 6, Jun. 2021, doi: 10.3390/pharmaceutics13060790.

[24] M. Naghdi *et al.*, “A green method for production of nanobiochar by ball milling-optimization and characterization,” *J Clean Prod*, vol. 164, pp. 1394–1405, Oct. 2017, doi: 10.1016/j.jclepro.2017.07.084.

[25] H. Zhang, C. Xu, W. Xiao, K. Ameyama, and C. Ma, “Enhanced mechanical properties of Al5083 alloy with graphene nanoplates prepared by ball milling and hot extrusion,” *Materials Science and Engineering: A*, vol. 658, pp. 8–15, Mar. 2016, doi: 10.1016/j.msea.2016.01.076.

[26] S. Aitipamula and R. B. H. Tan, “1. Pharmaceutical co-crystals: crystal engineering and applications,” in *Multi-Component Crystals*, De Gruyter, 2017, pp. 1–31. doi: 10.1515/9783110464955-001.

[27] A. Krusenbaum, S. Grätz, G. T. Tigineh, L. Borchardt, and J. G. Kim, “The mechanochemical synthesis of polymers,” Mar. 18, 2022, *Royal Society of Chemistry*. doi: 10.1039/d1cs01093j.

[28] D. Zhao, S. Yu, B. Sun, S. Gao, S. Guo, and K. Zhao, “Biomedical Applications of Chitosan and Its Derivative Nanoparticles,” *Polymers (Basel)*, vol. 10, no. 4, p. 462, Apr. 2018, doi: 10.3390/polym10040462.

[29] B. Li, J. Elango, and W. Wu, “Recent Advancement of Molecular Structure and Biomaterial Function of Chitosan from Marine Organisms for Pharmaceutical and Nutraceutical Application,” *Applied Sciences*, vol. 10, no. 14, p. 4719, Jul. 2020, doi: 10.3390/app10144719.

[30] N. Morin-Crini, E. Lichtfouse, G. Torri, and G. Crini, “Applications of chitosan in food, pharmaceuticals, medicine, cosmetics, agriculture, textiles, pulp and paper, biotechnology, and environmental chemistry,” Dec. 01, 2019, *Springer Verlag*. doi: 10.1007/s10311-019-00904-x.

[31] A. J. Jafari, S. Golbaz, and R. R. Kalantary, “Treatment of hexavalent chromium by using a combined fenton and chemical precipitation process,” *Journal of Water Reuse and Desalination*, vol. 3, no. 4, pp. 373–380, 2014, doi: 10.2166/wrd.2013.113.

[32] V. E. Pakade, N. T. Tavengwa, and L. M. Madikizela, “Recent advances in hexavalent chromium removal from aqueous solutions by adsorptive methods,” 2019, *Royal Society of Chemistry*. doi: 10.1039/c9ra05188k.

[33] S. Kang, G. Wang, H. Zhao, and W. Cai, “Highly efficient removal of hexavalent chromium in aqueous solutions *via* chemical reduction of plate-like micro/nanostructured zero valent iron,” *RSC Adv*, vol. 7, no. 88, pp. 55905–55911, 2017, doi: 10.1039/C7RA10846J.

[34] E. Majigsuren *et al.*, “Adsorption of Chromium (III) and Chromium (VI) Ions from Aqueous Solution Using Chitosan–Clay Composite Materials,” *Polymers (Basel)*, vol. 16, no. 10, May 2024, doi: 10.3390/polym16101399.

[35] W. S. W. Ngah and S. Fatinathan, “Adsorption characterization of Pb(II) and Cu(II) ions onto chitosan-tripolyphosphate beads: Kinetic, equilibrium and thermodynamic studies,” *J Environ Manage*, vol. 91, no. 4, pp. 958–969, Mar. 2010, doi: 10.1016/j.jenvman.2009.12.003.

[36] A. Rao, A. Kumar, R. Dhodapkar, S. Pal, and T. R. Cadaval, “Adsorption of five emerging contaminants on activated carbon from aqueous medium: kinetic characteristics and computational modeling for plausible mechanism,” 2014, doi: 10.1007/s11356-020-12014-1/Published.

[37] A. Pawlak and M. Mucha, “Thermogravimetric and FTIR studies of chitosan blends,” *Thermochim Acta*, vol. 396, no. 1–2, pp. 153–166, Feb. 2003, doi: 10.1016/S0040-6031(02)00523-3.

[38] Y. Lin, Y. Hong, Q. Song, Z. Zhang, J. Gao, and T. Tao, “Highly efficient removal of copper ions from water using poly(acrylic acid)-grafted chitosan adsorbent,” *Colloid Polym Sci*, vol. 295, no. 4, pp. 627–635, Apr. 2017, doi: 10.1007/s00396-017-4042-8.

[39] shimaa hamza, M. Elsawy, noha alian, and nihal shaker, “Synthesis and Evaluation of Performance Characteristics Green Composites from Sustainable Fatty Chitosan Graft Copolymer with Acrylic Acid for Wastewater Treatment,” *Egypt J Chem*, vol. 0, no. 0, pp. 0–0, May 2021, doi: 10.21608/ejchem.2021.73857.3656.

[40] W. Luo, Z. Bai, and Y. Zhu, “Fast removal of Co( <scp>ii</scp> ) from aqueous solution using porous carboxymethyl chitosan beads and its adsorption mechanism,” *RSC Adv*, vol. 8, no. 24, pp. 13370–13387, 2018, doi: 10.1039/C7RA13064C.

[41] L. Zhang, S. Tang, F. He, Y. Liu, W. Mao, and Y. Guan, “Highly efficient and selective capture of heavy metals by poly(acrylic acid) grafted chitosan and biochar composite for wastewater treatment,” *Chemical Engineering Journal*, vol. 378, Dec. 2019, doi: 10.1016/j.cej.2019.122215.

[42] M. A. H. Dhaif-Allah, S. N. Taqui, U. T. Syed, and A. A. Syed, “Kinetic and isotherm modeling for acid blue 113 dye adsorption onto low-cost nutraceutical industrial fenugreek seed spent,” *Appl Water Sci*, vol. 10, no. 2, Feb. 2020, doi: 10.1007/s13201-020-1141-3.

[43] K. Anwar *et al.*, “Application of Freundlich and Temkin Isotherm to Study the Removal of Pb(II) Via Adsorption on Activated Carbon Equipped Polysulfone Membrane,” 2018. [Online]. Available: www.sciencepubco.com/index.php/IJET

[44] A. Rao, A. Kumar, R. Dhodapkar, S. Pal, and T. R. Cadaval, “Adsorption of five emerging contaminants on activated carbon from aqueous medium: kinetic characteristics and computational modeling for plausible mechanism,” 2014, doi: 10.1007/s11356-020-12014-1/Published.